Review | Received 2 May 2026; Revised 2 June 2026; Accepted 4 June 2026; Published 18 June 2026
https://doi.org/10.55092/la20260002

Electrochemiluminescence biosensing of biomarkers and bioimaging of cellular functional molecules

Lele Li[1],†, Xue Dong[2],†, Qin Wei[2],* and Huangxian Ju[1],*

[1] State Key Laboratory of Analytical Chemistry for Life Science, School of Chemistry, Nanjing University, Nanjing 210023, China

[2] Key Laboratory of Interfacial Reaction and Sensing Analysis in Universities of Shandong, School of Chemistry and Chemical Engineering, Collaborative Innovation Center for Green Chemical Manufacturing and Accurate Detection, University of Jinan, Jinan 250022, China

† These authors contributed equally to this manuscript.

* Correspondence authors; E-mails: chm_weiq@ujn.edu.cn (Q.W.); hxju@nju.edu.cn (H.J.).

Highlights:

- Systematic overview of ECL luminophores from small molecules to frameworks.
- Advances in ECL biosensing for proteins, nucleic acids, and small molecules.
- ECL imaging of cellular secretions, membrane proteins, and intracellular molecules.
- Key challenges and future opportunities in ECL biosensing and imaging.

Abstract: Electrochemiluminescence (ECL) has emerged as a powerful analytical tool for the detection of biomarkers and the imaging of cellular functional molecules, owing to its low background, high sensitivity, and excellent spatiotemporal resolution. This review first summarizes representative classes of ECL luminophores, including organic small molecules, inorganic nanomaterials, and structurally programmable frameworks and polymers, along with their characteristic properties and recent applications. Subsequently, recent advances in ECL biosensing for *in vitro* detection of biomarkers such as proteins, nucleic acids, and small molecules are discussed, with particular attention to the evolution of target analytes and breakthroughs in achieving ultra-low detection limits. Next, this review focuses on the cutting-edge applications of ECL imaging at single-cell level. By integrating spatial confinement, label-free imaging, and *in situ* co-reactant generation with diverse signal-amplification strategies, ECL technology enables dynamic, minimally invasive, and high-resolution imaging of single-cell secretions, membrane proteins, and intracellular molecules, underscoring its potential for resolving functional heterogeneity at the single-cell level. Finally, the current challenges and future directions in ECL biosensing and imaging are outlined.

Keywords: electrochemiluminescence; ECL biosensing and imaging; biomarkers; cellular functional molecules; ECL luminophores

1. Introduction

Electrochemiluminescence (ECL) is an analytical technique in which the luminophores are driven to an excited state through electrochemical reactions to emit light signals [1]. By combining electrochemical controllability with optical sensitivity, ECL analysis offers near-zero background, high sensitivity, a wide dynamic range, and precise spatiotemporal control [2–4], making it highly attractive for biomarker detection and the imaging of cellular functions [5,6]. The performance of ECL technology is largely determined by its luminophores [7]. With rapid advances in nanomaterials and interfacial engineering, the family of ECL luminophores has expanded from conventional organic small molecules (e.g., tris(2,2'-bipyridine)ruthenium(II), $Ru(bpy)_3^{2+}$, and luminol) to inorganic nanocrystals [8–10], including quantum dots (QDs), metal nanoclusters, perovskites, and carbon nanomaterials, as well as structurally tunable frameworks and polymers such as metal-organic frameworks (MOFs), covalent organic frameworks (COFs), and aggregation-induced emission (AIE) materials [11–13]. These diverse material classes each offer unique advantages in luminescence efficiency, wavelength tunability, stability, and biocompatibility, collectively providing a rich material foundation for the construction of high-performance ECL biosensing platforms [14,15].

ECL biosensing couples these luminophores with selective recognition elements such as antibodies, aptamers, and nucleic acid probes [16,17], enabling sensitive and specific detection of proteins, nucleic acids, and small-molecule biomarkers with relatively simple instrumentation and rapid assay formats [18–20]. Driven by the advances in functional nanomaterials and by integration with microfluidics and imaging technologies, the scope of *in vitro* ECL biosensing has markedly expanded in recent years [21,22], extending from conventional *in vitro* detection of protein and nucleic acid biomarkers to high-precision imaging at the single-molecule, signal-cell and single-particle levels [23,24]. The convergence of ECL with microscopy has given rise to ECL imaging technology [25,26]. Unlike fluorescence-based methods, ECL technology does not require external photoexcitation and therefore avoids photobleaching and autofluorescence [27,28], making it a powerful tool for visualizing functional molecules in cells [29]. In single-cell analysis, ECL imaging has achieved a paradigm shift from ensemble-averaged measurements to single-entity precision imaging [30], enabling spatially resolved profiling of cellular secretions [31], *in situ* visualization of membrane proteins [32], and dynamic tracking of intracellular molecules [33]. These advances underscore its promise for dissecting cellular heterogeneity, signal transduction, and disease mechanisms [34,35]. By integrating advanced functional materials, precise interfacial engineering, and efficient imaging strategies [36], ECL technology is advancing towards higher sensitivity, higher throughput, and lower invasiveness, positioning itself as a key player in precision medicine, point-of-care diagnostics, and the study of dynamic life processes.

Unlike recent reviews that focus on nanomaterial-based ECL (where nanomaterials serve either as luminophore carriers or as the luminophores themselves) or on the construction of ECL biosensors [37–39], this review centers on the development of ECL luminophores and their applications in both *in vitro* biomarker detection and the bioimaging of functional cellular molecules at the single-cell level. The first part of this review summarizes representative ECL luminophores, including organic small molecules, inorganic nanomaterials, and structurally programmable frameworks and polymers, together with their key properties and recent applications. Then, ECL-based *in vitro* sensing of proteins, nucleic acids, and

small-molecule biomarkers is discussed, and the cutting-edge applications of ECL imaging in visualizing cellular functions at the single-cell level are described, including high-spatiotemporal-resolution imaging of cellular secretions, membrane proteins, and intracellular species. Finally, future opportunities and challenges in ECL biosensing and imaging are outlined, offering valuable insights for researchers and practitioners dedicated to advancing the next generation of ECL technologies.

2. ECL luminophores

ECL luminophores are the substances that participate in interfacial redox reactions at electrode surfaces to generate luminescent signals [40]. Based on the chemical composition, structural features, and emission mechanisms, they can be broadly divided into three categories: conventional organic small molecules (e.g., $Ru(bpy)_3^{2+}$ and luminol), inorganic nanomaterials (including semiconductor nanocrystals, clusters, and carbon-based materials), and structurally tunable frameworks and polymers such as MOFs, COFs, polymer dots (Pdots) and AIE materials. This section systematically summarizes the representative ECL luminophores in each category, along with their characteristic properties and recent applications.

2.1. Organic small-molecule luminophores

Organic small-molecule luminophores are the earliest and most extensively studied class of ECL materials. Their emission typically arises from radiative decay of excited-state species. Mechanistically, they can be divided into two main types. The first type, represented by metal complexes such as ruthenium and iridium compounds, involves emission through metal-to-ligand charge transfer (MLCT) [41]. The second type, exemplified by luminol and certain purely organic molecules, involves emission originating from intraligand or intramolecular π–π* or n–π* transitions [42]. These materials generally possess well-defined molecular structures, predictable redox potentials, and good synthetic tunability, enabling precise control over emission wavelength, solubility, and bioconjugation properties through molecular design [43].

2.1.1. $Ru(bpy)_3^{2+}$ and its derivatives

$Ru(bpy)_3^{2+}$ is the ECL "gold standard" luminophore [44]. In the presence of tri-n-propylamine (TPrA) as a coreactant, $Ru(bpy)_3^{2+}$ is oxidized to $Ru(bpy)_3^{3+}$, while TPrA is simultaneously oxidized to a strongly reducing radical intermediate. This intermediate reduces $Ru(bpy)_3^{3+}$ to the excited state $Ru(bpy)_3^{2+}$*, which subsequently relaxes to the ground state, producing orange-red emission at around 610 nm (Figure 1a) [45]. This system offers several notable advantages, including high emission efficiency, good electrochemical reversibility, and excellent stability [46]. By introducing reactive functional groups such as carboxyl groups, N-hydroxysuccinimide (NHS) esters, and biotin, a variety of $Ru(bpy)_3^{2+}$ derivatives have been prepared for covalent labeling of biomolecules, including antibodies and nucleic acids (Figure 1b) [47–50]. ECL immunoassays based on $Ru(bpy)_3^{2+}$/TPrA system have been successfully commercialized, as exemplified by the Roche Elecsys platform, and widely used for the highly sensitive detection of clinical biomarkers such as prostate-specific antigen (PSA), cardiac troponin, and alpha-fetoprotein (AFP). However, the relatively high cost of the $Ru(bpy)_3^{2+}$ luminophore and single emission wavelength limit its utility in multiplexed detection, which has driven the development of alternative luminophores such as iridium complexes.

2.1.2. Iridium complexes

To achieve multi-wavelength analysis, iridium complexes such as tris(2-phenylpyridine)iridium(III) ($Ir(ppy)_3$) and bis(2-phenylbenzothiazolato)(acetylacetonate)iridium(III) ($Ir(bt)_2(acac)$) have attracted considerable attention as wavelength-tunable organometallic luminophores [51]. Their ECL mechanism is similar to that of ruthenium complexes, but their stronger spin-orbit coupling affords higher phosphorescence quantum yields and longer excited-state lifetimes [52]. By modifying the cyclometalated ligands, such as phenylpyridine, phenylquinoline, and benzothiazole derivatives, the emission wavelength can be systematically tuned from green (approximately 510 nm) to red (approximately 620 nm) and even into the near-infrared region (Figure 1c) [53,54]. This tunability offers a clear advantage in multiplexed detection (Figure 1d). For example, green-emissive $Ir(ppy)_3$ and red-emissive tris(1-phenylisoquinoline)iridium(III) ($Ir(piq)_3$) have been used to label antibodies against two different tumor markers (Figure 1e), enabling simultaneous detection of carcinoembryonic antigen (CEA) and AFP on the same sensing interface without spectral crosstalk. In addition, some iridium complexes exhibit excellent electrochemical stability. At present, the main obstacles to broader application are their relatively high synthetic cost and the poor water solubility of some complexes. Future studies should focus on designing water-soluble ligands and developing lower-cost synthetic routes.

2.1.3. Luminol and its derivatives

Luminol is one of the earliest small-molecule ECL emitters identified. Its ECL behavior typically relies on hydrogen peroxide (H_2O_2) as a coreactant [55]. In alkaline solution, luminol is electrochemically oxidized at the electrode surface to form a diazaquinone intermediate, which subsequently reacts with reactive oxygen species (e.g., HO_2^-, $O_2^{-}\bullet$) generated from H_2O_2 decomposition (Figure 1f) [56–58]. This process produces the excited state of 3-aminophthalate, which emits blue light at approximately 425 nm upon relaxation. The luminol system offers several key advantages, including low cost, high quantum yield, and no reliance on precious metals. Its derivatives, such as N-(4-aminobutyl)-N-ethylisoluminol (ABEI), exhibit improved water solubility and labeling efficiency [59,60]. For instance, the aminobutyl side chain in ABEI enhances hydrophilicity and provides an additional amino group, facilitating covalent coupling to antibodies, nucleic acids, and other biomolecules via glutaraldehyde or 1-ethyl-3-(3-dimethylaminopropyl)carbodiimide (EDC)/NHS chemistry [61]. In practical applications, luminol/H_2O_2 systems are widely used in flow-injection analysis and the detection of glucose and other H_2O_2-related metabolites. For example, a flow-injection ECL system based on luminol/H_2O_2 has been successfully applied to the simultaneous determination of lactate and cholesterol in clinical serum samples, enabling high-throughput analysis with good agreement to results from standard clinical biochemical analyzers [62]. Despite these advantages, this system requires a relatively high working potential, which is susceptible to interference from electroactive species in complex matrices, and often suffers from rapid signal decay, limiting its use in long-term kinetic monitoring. Moreover, its alkaline operating environment (pH 9.0–10.5) is incompatible with physiological conditions (pH 7.4), restricting its application in live-cell and *in vivo* analysis. Current efforts are therefore focused on developing physiologically compatible derivatives, such as L012 (8-amino-5-chloro-7-phenylpyrido[3,4-d]pyridazine-1,4(2H,3H)-dione, a luminol derivative), and on optimizing strategies to improve signal stability.

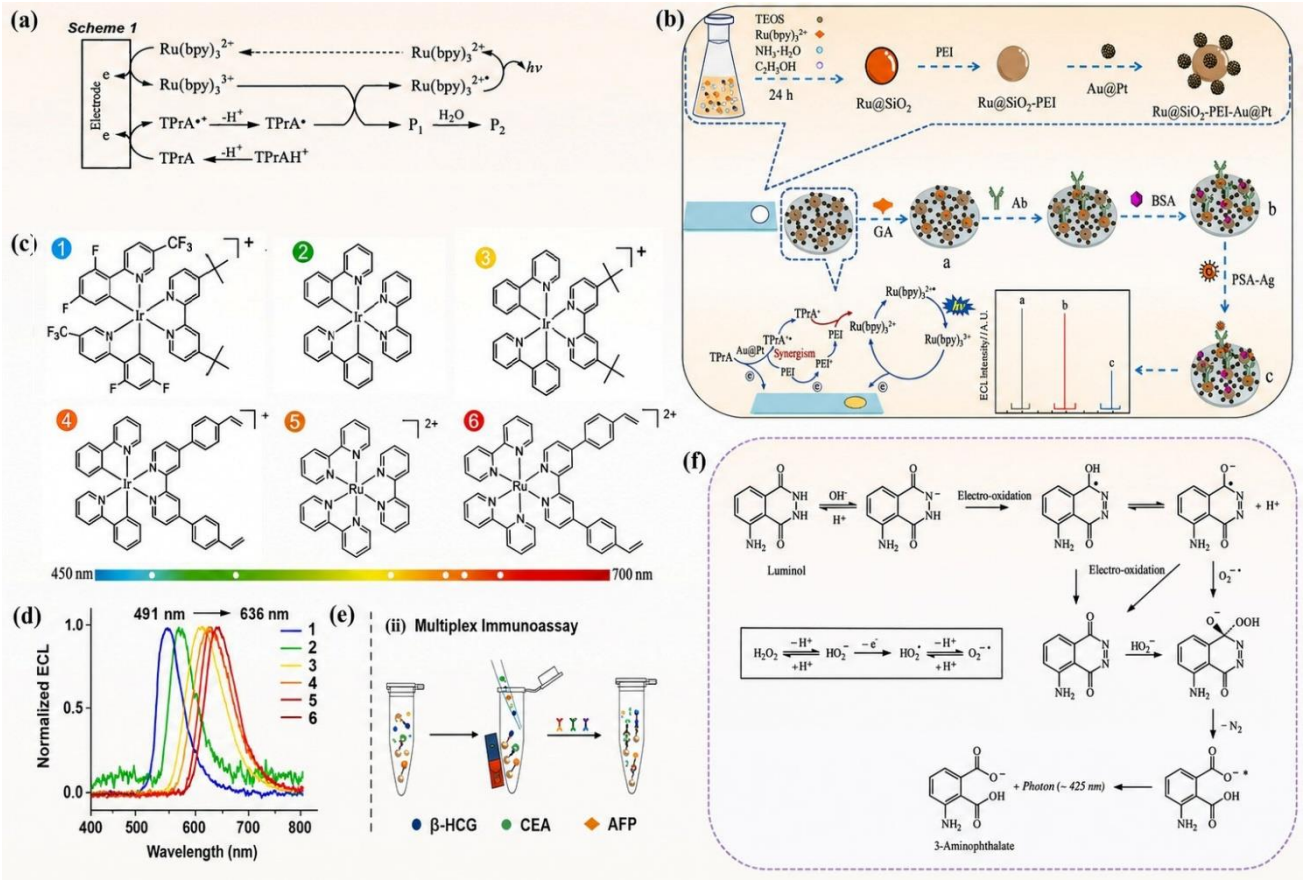

Figure 1. Representative ECL systems and mechanisms. **(a)** Mechanism for $Ru(bpy)_3^{2+}$/TPrA ECL system. Reprinted with permission [45]. Copyright 2002 American Chemical Society; **(b)** Schematic diagram of the ECL immunosensor based on Ru@SiO_2-PEI-Au@Pt. Reprinted with permission [49]. Copyright 2026 Wiley-VCH; **(c)** Molecular structures of $Ir(dFCF_3ppy)_2(dtbbpy)^+$, $Ir(ppy)_3$, $Ir(ppy)_2(dtbbpy)^+$, $Ir(ppy)_2(dvbpy)^+$, $Ru(bpy)_3^{2+}$ and $Ru(bpy)_2(dvbpy)^{2+}$ (1–6); **(d)** Normalized ECL spectra of the six luminophores; **(e)** Schematic diagram of the multiplex immunoassay based on iridium complexes. Reprinted with permission [54]. Copyright 2018 American Chemical Society; **(f)** Proposed mechanism for the ECL reaction of luminol. Reprinted with permission [57]. Copyright 1999 Elsevier Science B.V.

2.1.4. Other organic small molecules (e.g., phenothiazines)

In addition to the metal complexes described above, certain purely organic small molecules also exhibit intrinsic ECL activity, with phenothiazine derivatives emerging as a particular research focus in recent years [63]. Representative compounds include phenothiazine (PTZ), methylphenothiazine (MPTZ), N-phenylphenothiazine (PTH), and their substituted derivatives. Their ECL emission originates from the reversible formation of radical cations: anodic oxidation generates a stable radical cation, which then undergoes electron-transfer annihilation with the neutral reduced form to produce an excited state that emits light [64]. A major advantage of phenothiazine-based luminophores is the absence of metal centers, which reduces biological toxicity, while their redox potentials can be flexibly tuned via substituent effects [65]. For example, the oxidation potential of PTZ is approximately +0.85 V *vs.* Ag/Ag^+, whereas introducing two methoxy groups at 3,7-positions of the phenothiazine skeleton lowers the potential of the resulting derivative, DMOP-PTZ, to +0.52 V, corresponding to a decrease of 0.33 V. This shift

facilitates ECL excitation at lower potentials and minimizes electrochemical damage to biological samples [66]. Additionally, some phenothiazine derivatives combine electrochromic and ECL functionalities, making them attractive for constructing smart sensors [67]. Currently, the main limitations to their broader application are relatively low emission efficiency and insufficient long-term stability. Future efforts will likely focus on the structural design of high-performance derivatives, MOF/COF-based confinement-enhancement strategies, and improved water solubility, aiming to advance their practical use in low-cost, low-toxicity ECL biosensing.

2.2. Inorganic nanomaterial luminophores

Inorganic nanomaterial luminophores predominantly comprise nanostructured semiconductor and metallic materials, including QDs, perovskites, metal nanoclusters (NCs), and carbon dots (CDs). Unlike molecular organic luminophores, the ECL properties of inorganic nanomaterial luminophores are fundamentally governed by nanoscale physical phenomena, such as the quantum confinement effect, surface defect states, and discrete molecular orbital energy levels. These attributes confer distinct advantages, including the ability to achieve continuous and precise wavelength tuning by modulating particle size and composition [68,69]. Furthermore, most inorganic luminophores exhibit superior photostability and robust resistance to photobleaching, while specific materials like CDs and gold clusters demonstrate enhanced biocompatibility. These features collectively enable the development of multicolor ECL platforms and novel sensing systems for *in vivo* analysis.

2.2.1. Quantum dots

Semiconductor QDs, such as CdSe, CdTe, and PbS, are inorganic nanocrystals typically ranging from 2 to 10 nm in size [70–74]. Their ECL emission originates from the radiative recombination of "electron-hole pairs", yielding emission wavelengths that are continuously tunable from the ultraviolet to the near-infrared spectrum by adjusting particle size. This intrinsic size-color correspondence provides a natural advantage for multicolor ECL sensing applications. In the presence of co-reactants like potassium persulfate ($K_2S_2O_8$) or TPrA, QDs facilitate the alternating injection of electrons and holes at the electrode surface to generate excitons, which subsequently undergo radiative decay. Compared to organic complexes, QD-based ECL systems offer higher photostability, superior anti-photobleaching performance, and broader excitation spectra. However, the heavy metal toxicity associated with traditional cadmium-based QDs has limited their broader application in *in vivo* and cellular diagnostics. Consequently, the development of non-toxic or low-toxicity QDs, including $CuInS_2$, Ag_2S, and ZnS, has emerged as a major research frontier in recent years [75–77].

2.2.2. Perovskite materials

Perovskite materials, characterized by their unique ABX_3 structure (e.g., $CsPbBr_3$), have emerged as highly promising optoelectronic candidates in the field of ECL [78,79]. These materials exhibit exceptional carrier mobility, narrow emission profiles with a full width at half maximum (FWHM) of less than 30 nm, and bandgaps that are precisely tunable via halide ion exchange. In the ECL process, perovskite nanocrystals undergo electrochemical carrier injection at the electrode surface, followed by radiative exciton recombination. A significant advantage of these materials is their low onset potential, which typically

ranges from 0.2 to 0.3 V lower than that of the conventional $Ru(bpy)_3^{2+}$, thereby facilitating the reduction of background interference. Nevertheless, perovskites are inherently sensitive to moisture and oxygen, which leads to suboptimal stability during aqueous ECL detection. To address this challenge, current research focuses on enhancing aqueous stability through various strategies, including polymer encapsulation, silica coating, and ligand engineering. Researchers have innovatively assembled all-inorganic $CsPbBr_3$ nanocrystals *in situ* within the pores of a hydrophobic and highly crystalline imine-based covalent organic framework (COF-LZU1). The COF scaffold effectively isolates moisture and oxygen due to its hydrophobic architecture, markedly improving both the operational and long-term storage stability of $CsPbBr_3$ for aqueous ECL applications. This approach was successfully utilized to develop a high-performance ECL sensing platform for T-2 toxin detection (Figure 2a,b) [80]. Additionally, all-inorganic perovskites ($CsPbX_3$) generally exhibit superior thermal stability compared to their organic–inorganic hybrid counterparts, making them robust candidates for non-aqueous ECL sensing systems.

2.2.3. Metal nanoclusters

Metal NCs are composed of a precise assembly of several to dozens of metal atoms, such as gold, silver, or copper [81–85]. With dimensions typically below 2 nm, these clusters exhibit discrete, molecule-like electronic energy levels. Representative examples include glutathione-protected gold nanoclusters (GSH-AuNCs) and mercaptopropionic acid-stabilized silver nanoclusters (AgNCs). The ECL of metal nanoclusters (MNCs) originates from electronic transitions between highest occupied molecular orbital (HOMO) and lowest unoccupied molecular orbital (LUMO) levels rather than from surface plasmon resonance effects. These materials are characterized by large Stokes shifts exceeding 100 nm, prolonged luminescence lifetimes in the microsecond range, and excellent biocompatibility. In the presence of co-reactants, MNCs can generate either anodic or cathodic ECL signals. Notably, the ECL performance of MNCs is highly sensitive to the state of their surface ligands. Research involving ligand exchange between THPC-AuNCs and 8-mercaptooctanoic acid (MOA) revealed that ECL intensity initially increases as MOA replaces THPC due to a narrowed bandgap. The intensity subsequently decreases as the ligand shell undergoes reconstruction and the bandgap partially recovers. This dynamic evolution demonstrates the precise regulation of electronic band structures and ECL emission by surface ligands, providing a powerful tool for elucidating previously ambiguous mechanisms of ligand influence (Figure 2c) [86]. Due to their ultra-small size, MNCs readily penetrate cell membranes and have shown significant potential for cellular imaging and subcellular localization. However, the primary challenges for MNC-based ECL remain the relatively low absolute quantum yields, which are typically less than 1%, and the incomplete understanding of the mechanisms by which ligands dictate ECL performance.

2.2.4. Carbon nanomaterials

Carbon-based nanomaterials, including graphene QDs (GQDs) and CDs, represent a class of environmentally friendly ECL luminophores [87–90]. CDs, in particular, have garnered significant interest due to their facile synthesis, as well as their abundant surface functional groups and excellent aqueous solubility. The ECL emission of CDs is primarily attributed to electronic transitions involving surface defect states or the carbon core, typically necessitating the use of $K_2S_2O_8$ as a cathodic co-reactant. Compared to metallic QDs, CDs exhibit substantially lower cytotoxicity, making them highly suitable

for live-cell and *in vivo* ECL analysis. Furthermore, strategies such as nitrogen doping can enhance their ECL efficiency by more than an order of magnitude. Despite these advantages, CDs generally face challenges such as broad emission profiles (FWHM > 80 nm) and relatively low quantum yields compared to cadmium-based QDs. To circumvent the dependence on high concentrations of exogenous co-reactants, recent research has focused on the development of intelligent, self-supplying reactive oxygen species (ROS) systems. One such study reported a composite comprising luminol-derived CDs and a zinc-based metal-organic framework (Zn-MOF). This system leverages the "metal-framework charge transfer" effect to generate ROS *in situ* without the need for external oxidants. Additionally, the confined space of the MOF stabilizes luminescent intermediates, achieving a dual enhancement of ECL intensity and stability in near-neutral media (Figure 2d–h) [91]. This work offers a new paradigm for optimizing CD-based ECL performance through the synergistic modulation of surface states and local microenvironments. Future research is expected to focus on atomically precise doping and refined surface state engineering to further improve ECL efficiency, color purity, and operational stability.

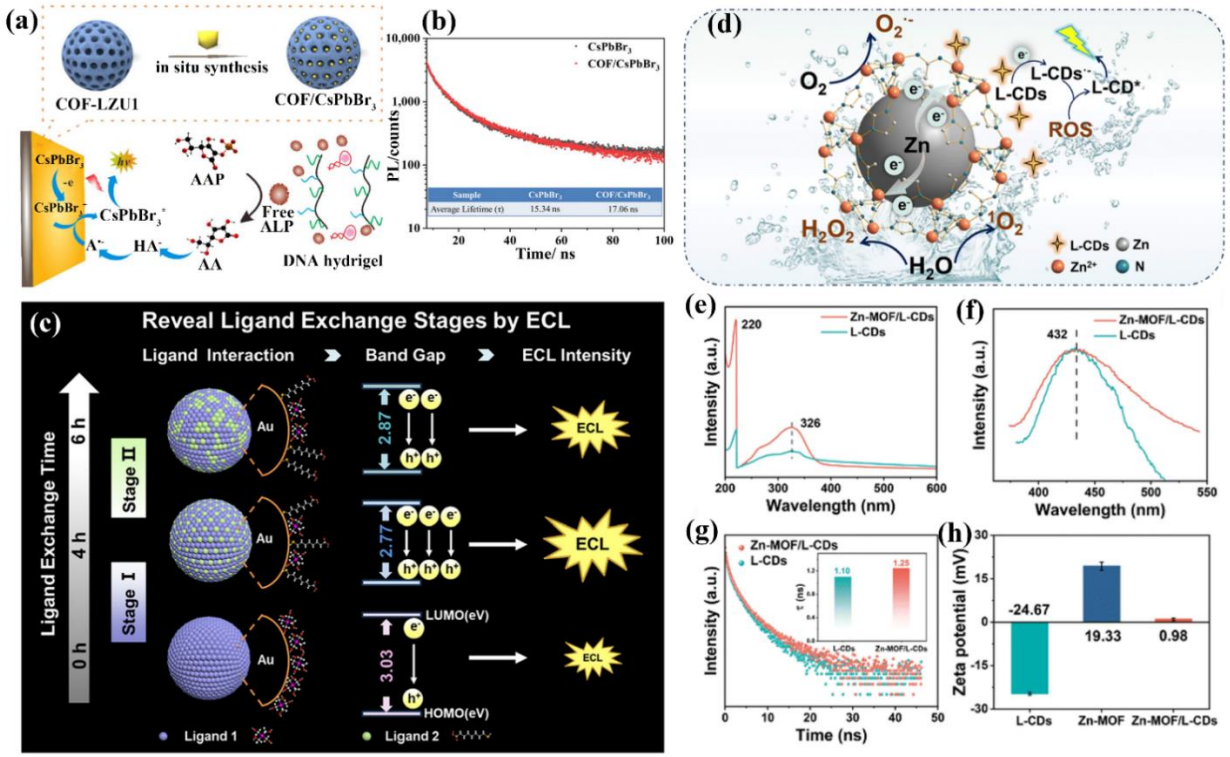

Figure 2. Inorganic nanomaterial luminophores designs for sensing platforms. **(a)** Schematic illustration of the preparation of COF-LZU1/$CsPbBr_3$ composite and its ECL response mechanism; **(b)** Time-resolved fluorescence decay curves of $CsPbBr_3$ and COF/$CsPbBr_3$. Reprinted with permission [80]. Copyright 2024 American Chemical Society; **(c)** Schematic Diagram of Monitoring Ligand Exchange Stages of AuNCs by ECL. Reprinted with permission [86]. Copyright 2025 American Chemical Society; **(d)** A schematic diagram of the mechanism of self-releasing ROS enhancing ECL based on the MMCT characteristics of Zn-MOF; **(e)** UV-vis spectra of luminol-derived carbon dots（L-CDs) and Zn-MOF/L-CDs; **(f)** Fluorescence emission spectra of L-CDs and Zn-MOF/LCDs under an excitation wavelength of 364 nm; **(g)** TRPL spectra of LCDs and Zn-MOF/L-CDs; **(h)** Zeta potential of L-CDs, Zn-MOF, and Zn MOF/L-CDs. Reprinted with permission [91]. Copyright 2026 Royal Society of Chemistry.

2.3. Porous framework and polymer-based luminophores

The integration of ECL units into periodic frameworks or conjugated polymer chains imparts unique spatial confinement effects, signal amplification capabilities, and distinct aggregation-state luminescent behaviors. The primary advantages of these materials stem from the performance synergy facilitated by their designable and extended architectures [92–95]. Specifically, the ordered topologies provide a unique confined microenvironment for luminescent centers, which not only stabilizes excited states to improve efficiency but also enhances sensing selectivity through pre-concentration effects. Furthermore, the extended conjugated systems, such as conjugated polymer chains, exhibit "molecular wire" characteristics that enable rapid charge delocalization and subsequent signal amplification. Finally, the aggregation behavior of these materials effectively leverages luminescence enhancement at high concentrations, successfully circumventing the traditional challenge of aggregation-caused quenching (ACQ).

2.3.1. MOF/COF

MOFs and COFs are crystalline porous materials characterized by periodic channel structures. As ECL luminophores, they function through two primary pathways. The first involves the direct construction of frameworks using ECL-active organic ligands, such as $Ru(bpy)_3^{2+}$ derivatives or porphyrins, to create three-dimensionally ordered arrays of luminescent centers [96]. Alternatively, traditional ECL emitters can be encapsulated within MOF/COF channels, where pore confinement effects enhance both luminescent efficiency and stability [97]. Lanthanide-organic frameworks (Ln-MOFs) are particularly noteworthy in this context. Complexes involving Eu^{3+} and Tb^{3+} exhibit characteristic narrow-band emissions—near 615 nm for Eu^{3+} and 545 nm for Tb^{3+}—alongside millisecond-scale luminescence lifetimes. These properties enable the effective elimination of background fluorescence interference through time-resolved techniques. A prominent research frontier focuses on integrating both luminescent centers and co-reaction functionalities into a single MOF architecture to simplify sensing systems. A europium-based MOF (ZL-2) was developed using 1,10-phenanthroline and carbonate ions (CO_3^{2-}) as ligands. During electrochemical oxidation, the CO_3^{2-} ligands are converted *in situ* into hydroxyl radicals (OH·), which serve as endogenous co-reactants to drive self-ECL without exogenous reagents. This ligand configuration also induces geometric distortion of the coordination environment, triggering the typically forbidden $^5D_0 \rightarrow {}^7F_4$ electric dipole transition. Consequently, the material exhibits exceptional deep red/near-infrared self-luminescence, providing new insights for developing self-powered, long-wavelength ECL materials (Figure 3a–d) [98]. The primary advantages of MOF/COF-based ECL luminophores reside in their high specific surface areas and designable pore environments. These features offer abundant active sites for target molecule capture, which is particularly advantageous for gas sensing and integrated capture-and-detection platforms. Nevertheless, current challenges include the limited conductivity of framework materials and their insufficient long-term structural stability in aqueous media.

2.3.2. Conjugated polymers

Conjugated polymers represent a class of organic macromolecules characterized by their π–π conjugated backbones [99–101]. During the ECL process, these materials exhibit a unique "molecular wire" effect. In this mechanism, electrochemically injected charge carriers migrate rapidly along the conjugated polymer backbone. Consequently, a single excitation event can trigger multiple luminescent units across the polymer segment, resulting in significant signal amplification. Furthermore, the ECL emission wavelengths of conjugated polymers can be systematically tuned from the visible to the near-infrared range through rational backbone modification and side-chain engineering. A representative material, poly(9,9-dioctylfluorene) (PFO), generates efficient ECL in the presence of the co-reactant TPrA. Its excellent film-forming capability also facilitates the fabrication of solid-state ECL devices. However, the widespread utility of these polymers remains hindered by the dual challenges of aggregation-induced luminescence quenching and sluggish thin-film ion transport, which collectively constrain the overall performance of the resulting devices.

2.3.3. Aggregation-induced emission materials

AIE materials provide a novel paradigm for overcoming the ACQ typically observed in traditional ECL luminophores [102–104]. Representative AIE-ECL emitters include tetraphenylethylene (TPE) derivatives, triphenylamine derivatives, and certain Schiff base complexes. In dilute solutions, these molecules exhibit extremely weak ECL signals because unrestricted intramolecular rotation allows excited-state energy to dissipate through non-radiative pathways. However, in the aggregated or solid state, the restriction of intramolecular rotation (RIR) activates radiative transition channels, which can enhance ECL intensity by dozens or even hundreds of times. This unique characteristic makes AIE materials particularly suitable for constructing biosensors with high-density labeling, as they eliminate the risk of self-quenching. A highly effective strategy for further boosting AIE-ECL efficiency involves utilizing the nano-confinement effect to construct integrated "nanoreactors". An efficient AIE nano-confined reactor was developed by *in situ* encapsulating TPE molecules within the pores of an NH_2-MIL-88 framework containing atomically dispersed iron catalytic sites. In this system, the MOF framework serves as a matrix to stabilize the aggregated state of the AIE molecules. Meanwhile, the internal Fe catalytic centers efficiently convert the $K_2S_2O_8$ co-reactant into active radicals *in situ*. This spatial confinement significantly shortens the transport distance between active species and luminescent molecules. Furthermore, the modified local kinetic and thermodynamic environments lower the reaction energy barriers. These factors synergistically achieve ultra-strong amplification of the AIE-ECL signal, leading to its successful application in the ultrasensitive sensing of cardiac troponin I (Figure 3e–i) [105]. Additionally, some AIE materials exhibit bidirectional ECL emission under both positive and negative potentials, which facilitates the development of self-calibrating sensors. While the AIE-ECL field is in a phase of rapid development, primary research directions currently include the design of aqueous AIE-ECL systems and the development of emitters with near-infrared emission. Future work will also focus on verifying their performance in multi-site labeling immunoassays.

The trajectory of ECL luminophore development has transitioned from conventional molecular species, such as $Ru(bpy)_3^{2+}$ and luminol, to functional nanocrystals, and finally to structurally designable frameworks and polymers. Leveraging unique luminescent mechanisms and physicochemical properties,

these diverse material classes offer distinct advantages in terms of sensitivity, wavelength tunability, stability, and biocompatibility. Collectively, they have expanded the performance boundaries of ECL sensing technology. The hybridization of cross-category materials—exemplified by the encapsulation of AIE units within MOFs or the integration of QDs with CDs—represents a promising frontier. When combined with the deep integration of luminescent mechanisms and sensing strategies, these advancements are poised to foster a new generation of high-performance ECL luminophores. Such innovations will ultimately address the increasingly sophisticated detection requirements within the field of bioanalysis.

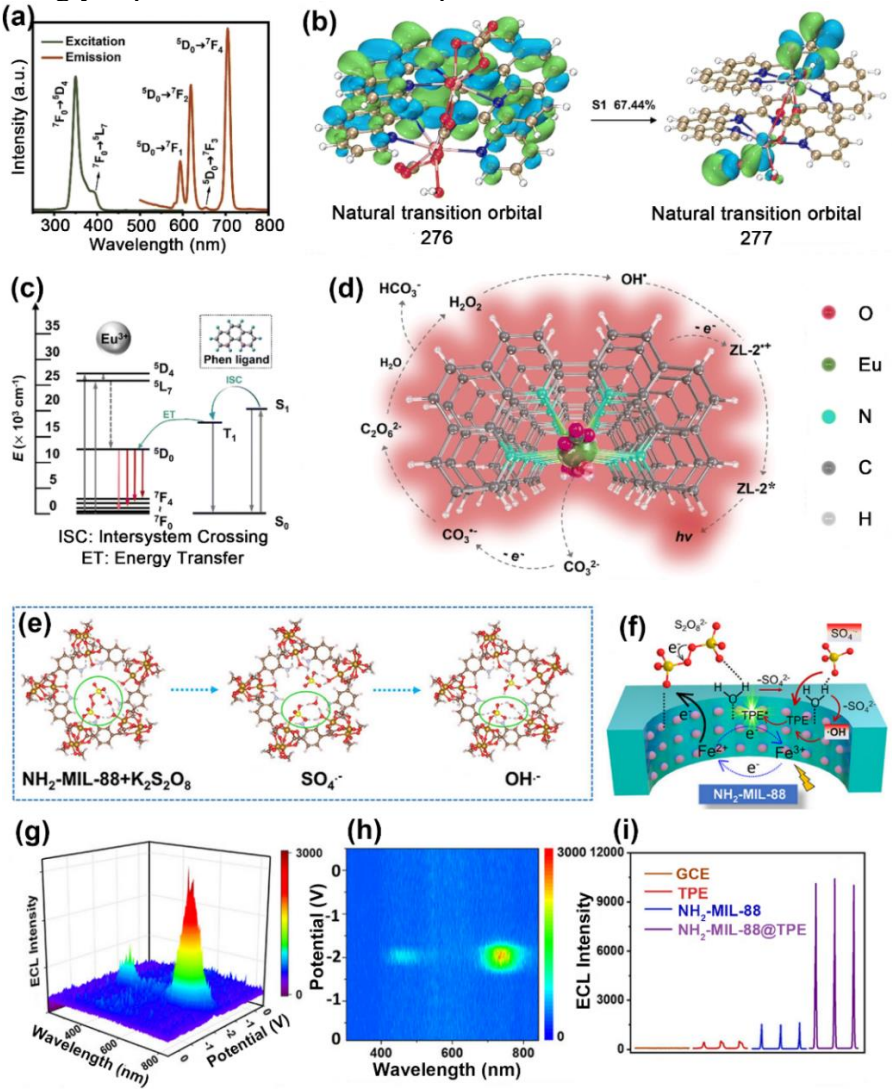

Figure 3. Porous framework luminophores designs for sensing platforms. **(a)** Excitation and emission spectra of europium-based MOF (Eu-MOF); **(b)** Natural transition orbital isodensity surfaces of S1 for Eu-MOF clusters; **(c)** Simple model for the energy transfer processes of the phenanthroline (Phen) ligand to Eu^{3+} and the f-f transition emission mechanism of Eu^{3+} in Eu-MOF; **(d)** Schematic diagram of the deep-red self-ECL mechanism in Eu-MOF. Reprinted with permission [98]. Copyright 2025 Royal Society of Chemistry; **(e)** The adsorption model in the catalysis of $K_2S_2O_8$ into free radicals on the nanoconfined NH_2-MIL-88; **(f)** The proposed aggregation-induced ECL (AIECL) mechanism in the nanoconfined NH_2-MIL-88; **(g)** The 3D ECL spectral image of NH_2-MIL-88@TPE; **(h)** 3D heat map image of NH_2-MIL-88@TPE; **(i)** the ECL of glassy carbon electrode, bare TPE, NH_2-MIL-88 and NH2-MIL-88@TPE in the presence of $K_2S_2O_8$. Reprinted with permission [105]. Copyright 2025 Wiley-VCH.

3. *In vitro* ECL biosensing and bioanalysis

Owing to the quick development of high-performance ECL luminophores and their integration with specific recognition elements such as antibodies, aptamers, or nucleic acid probes, ECL biosensing for biomarkers has been extensively applied [106–108]. Characterized by near-zero background noise, a wide dynamic range, and superior spatiotemporal resolution, ECL biosensing technology has emerged as a formidable tool for the analysis of complex biological specimens [109–111]. In recent years, the application landscape of *in vitro* ECL biosensing has expanded significantly, driven by the precision customization of functional nanomaterials and the integration of microfluidic systems and advanced imaging. This evolution has allowed the field to move beyond conventional biomarker detection for proteins and nucleic acids, reaching the frontier of precision imaging at the single-molecule and single-particle levels [71,112–114]. Consequently, this section systematically reviews the recent advancements in *in vitro* ECL biosensing, focusing on the dual dimensions of the evolution of target analytes and the fundamental breakthroughs in achieving ultra-low detection limits.

3.1. Detection of protein biomarkers

The highly sensitive and specific detection of protein biomarkers serves as the bedrock of clinical diagnosis. To achieve precise quantification of low-abundance proteins, the research frontier has focused on two primary objectives. The first objective involves the development of novel, high-performance ECL luminophores to provide more robust and stable signal sources. The second objective is the optimization of sensing interfaces to ensure efficient target capture and signal transduction. Recently, the implementation of sophisticated structural designs to modulate aggregation states, local microenvironments, and interfacial reaction kinetics has emerged as a critical strategy for significantly enhancing ECL sensing performance [87,115–118].

Rational molecular and supramolecular engineering of luminescent materials represents the fundamental pathway to overcome their intrinsic performance limitations. Through microfluidic technology, molecules with distinct luminescent properties can be precisely assembled into supramolecular nanoaggregates. This approach effectively utilizes an AIE molecular matrix to disperse and stabilize high-quantum-yield luminophores, which not only circumvents ACQ but also achieves highly efficient co-emission through inter-component synergy, providing robust signaling tags for immunoassay [119]. Furthermore, in-depth investigations into the mechanisms underlying performance enhancement can drive more rational material designs. Organic nanoparticles with specific surface defect states have been prepared via molecular engineering. Advanced techniques such as scanning electrochemical microscopy were then employed to quantify their interfacial charge transfer kinetics *in situ*, experimentally revealing the facilitative role of defect states in the ECL process and guiding the development of high-performance luminophores for Alzheimer's-related protein detection [120]. In addition to direct material modification, optimizing the local reaction microenvironment can significantly enhance signals from a kinetic perspective. Integrated “nanoreactors” have been constructed by encapsulating AIE molecules within MOFs possessing catalytic sites. This architecture enables the highly efficient *in situ* generation and utilization of reactive species within a confined space, which substantially amplifies ECL intensity and has been successfully applied to the ultrasensitive detection of cardiac troponin I [105]. However, despite possessing powerful signal sources, detection performance in complex biological samples

remains a significant challenge. Therefore, constructing anti-fouling biological interfaces that combine high sensitivity with high selectivity is a critical step for translating high-performance materials into practical applications. By integrating zwitterionic chemistry with ECL sensing, bifunctional "recognition-anti-fouling" interfaces can be established on nanocomposite substrates. These interfaces effectively repel non-specific adsorption with minimal loss of ECL efficiency, enabling label-free, highly selective monitoring of targets such as tumor exosomes and significantly improving methodological reliability (Figure 4) [121]. Following the resolution of issues regarding signal generation and interfacial specificity, the functionality of ECL sensing is expanding toward systematic diversification, integration, and green chemistry. On one hand, researchers have innovatively combined sensing with information encryption by creating dynamic, multi-level encrypted interfaces using functional inks. In this system, biological recognition, electrochemical stimulation, and catalytic reaction sequences collectively serve as decryption "keys" for the secure reading of biological information and dual-mode detection of cancer biomarkers [122]. On the other hand, reducing dependence on toxic exogenous reagents through the development of environmentally friendly endogenous reaction systems is another vital direction. By precisely designing alloy nanocatalysts to utilize endogenous dissolved oxygen as a co-reactant, green and efficient ECL sensing platforms have been established for human epidermal growth factor receptor 2 (HER2) protein analysis, offering new perspectives for future long-term monitoring and even *in vivo* analysis [123].

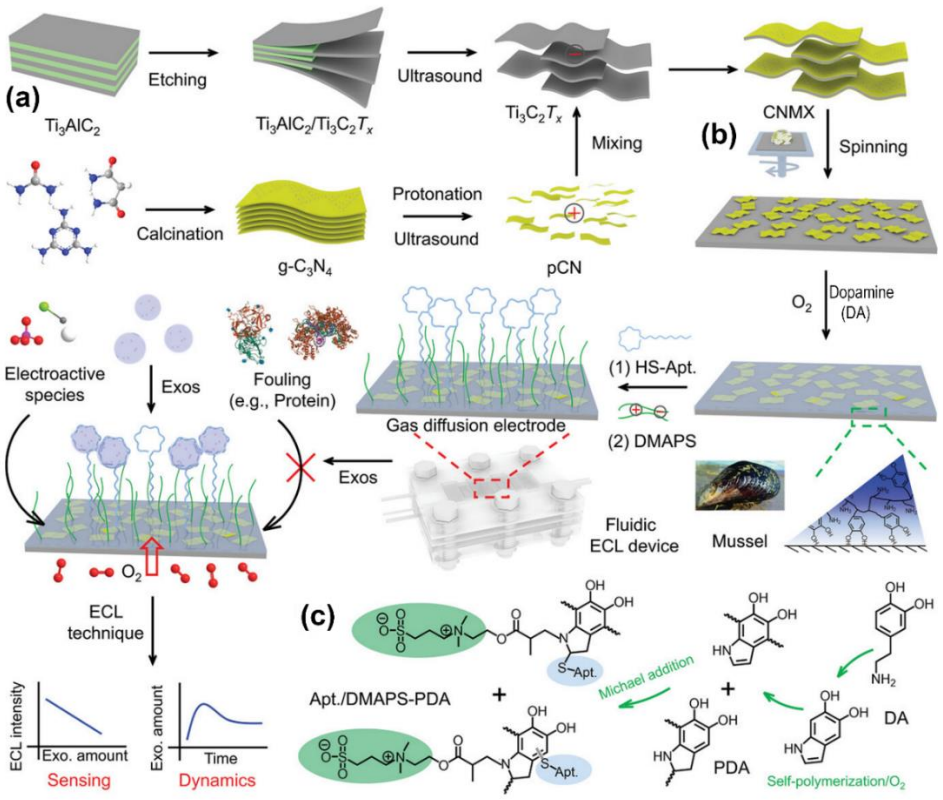

Figure 4. Construction of the sensing platform for protein biomarkers. **(a)** Synthesis process of graphitic carbon nitride (g-C_3N_4) nanosheets and $Ti_3C_2T_x$ MXene nanosheets (CNMX); **(b)** Construction process of aptamer/3-dimethyl (methacryloyloxyethyl) ammonium propane sulfonate polydopamine (DMAPS-PDA) assaying surface for Exos sensing and dynamics tracking using a homemade fluidic ECL device; **(c)** Mechanisms for the nonfouling and sustainable organic layer formation. Reprinted with permission [121]. Copyright 2023 Wiley-VCH.

3.2. Detection of nucleic acid biomarker

The primary challenge in detecting nucleic acid biomarkers lies in achieving precise, single-base differentiation of ultralow-abundance target sequences to support rapid and convenient point-of-care diagnostics. While traditional nucleic acid amplification techniques offer high sensitivity, they are often hindered by cumbersome procedures and a high risk of contamination. Consequently, developing amplification-free direct ECL detection strategies has become a frontier direction in this field. Current research focuses on three primary areas: signal source enhancement, target-triggered cascaded amplification, and the construction of integrated detection platforms [124–128]. These efforts aim to bridge the gap between laboratory detectability and practical, precise clinical testing.

Constructing high-brightness ECL signal sources is fundamental to improving the raw signal-to-noise ratio and bypassing the need for amplification. Research in this area emphasizes not only the luminescence efficiency of materials but also their compatibility with nucleic acid sensing interfaces. DNA nanosheet templates have been utilized to guide the self-assembly of perovskite QDs into two-dimensional superlattices. In this design, the surface DNA structures serve as direct interfaces for molecular recognition and immobilization. This achieves a monolithic integration of signal materials and bioprobes, providing a foundation for stable and efficient sensing [129]. Furthermore, fine-tuning the microstructure of MOFs enables the simultaneous catalysis of endogenous co-reactants and the immobilization of nucleic acid probes. This synergy between signal generation and the recognition interface significantly simplifies the detection system [130,131]. Second, implementing efficient signal transduction and amplification mechanisms at the sensing interface is critical for addressing low-abundance targets. Various isothermal amplification strategies based on enzyme catalysis or DNA nanomachines have been developed for nucleic acid markers. By integrating multicolor ECL luminophores with DNA walker technology, researchers can perform parallel and visual analysis of multiple genetic targets on a single electrode array. This approach utilizes DNA cycling for signal amplification and spatial resolution to enhance the throughput and convenience of multiplexed detection, making it ideal for joint screening scenarios [132]. Another strategy focuses on system simplification through “all-in-one” nanotags that combine ECL luminescence with enzyme-like catalytic activity. These tags support a dual-mode platform for colorimetric pre-screening and ECL quantification. Such systems achieve rapid and sensitive detection without additional enzymes or amplification, thereby expanding the technology’s practical utility (Figure 5) [133]. Finally, system-level integration and innovation have become central to applications in bedside diagnostics and resource-limited settings. This transition requires the miniaturization and automation of complex sample processing, target enrichment, and detection steps. Integrating active enrichment techniques, such as alternating current electro-osmotic flow, with microfluidic chips allows for the direct transport of nucleic acids from unprocessed clinical samples like saliva to the sensing interface. This process can complete an entire assay within minutes, offering a robust tool for real-time diagnostics [134]. These full-chain innovations—spanning materials, methodologies, and systems—are driving ECL nucleic acid sensing from sophisticated laboratory analysis toward broad and practical clinical application.

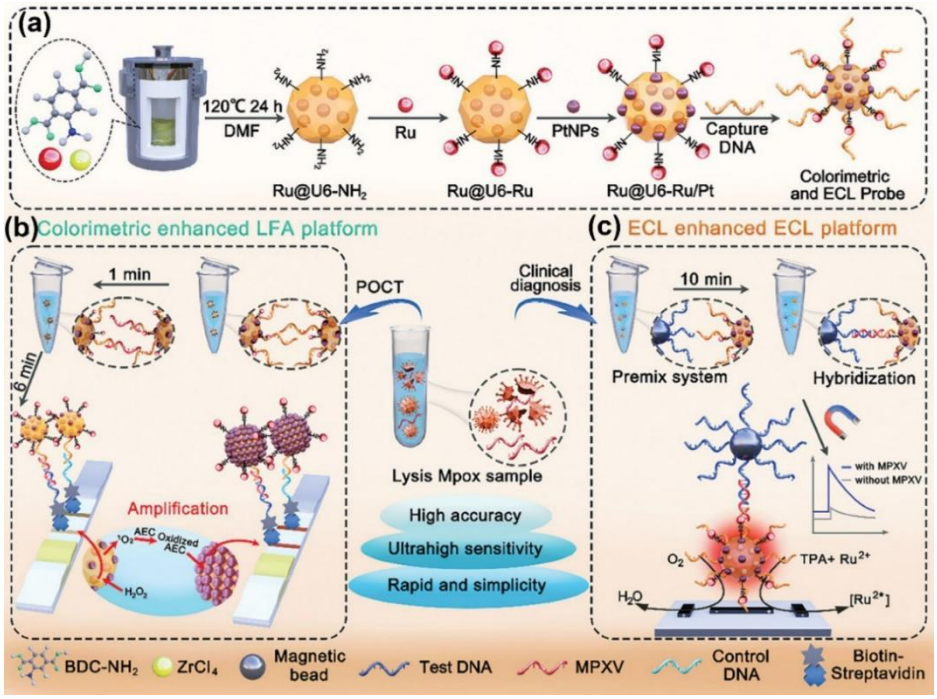

Figure 5. Construction of the sensing platform for nucleic acid biomarkers. **(a)** Schematic illustration of synthesis of Ru@U6-Ru/Pt as the dual-signal probe; **(b)** Schematic illustration of colorimetric enhanced Ru@U6-Ru/Pt NPs based LFA; **(c)** Schematic illustration of Ru@U6-Ru/Pt NPs-based ECL sensing platform. Reprinted with permission [133]. Copyright 2024 Wiley-VCH.

3.3. Detection of small-molecule biomarker

Small-molecule biomarkers, including neurotransmitters, metabolites, and energy-related molecules, serve as indispensable indicators of physiological homeostasis and disease progression [135,136]. To achieve high-sensitivity analysis within complex biological matrices, the research focus has transitioned from empirical luminophore screening to precision molecular tailoring, micro-regulation of aggregation states, and the innovation of interfacial reaction pathways [137–140].

Molecular engineering serves as the cornerstone for enhancing sensing performance. By designing novel donor-acceptor architectures, such as V-shaped organic molecules incorporating carbazole and pyridine, electronic energy levels can be optimized at the source. This strategy improves cathodic luminescence efficiency, enabling wide-range epinephrine analysis through a “signal quenching” mode [141]. Beyond skeletal design, extending conjugation via terminal phenyl rings and synergistically optimizing solvent microenvironment polarity can effectively balance AIE with ACQ. This optimization maximizes signal output for melatonin sensors in their ideal aggregation states [142]. Such regulation has further evolved into precision assembly at the molecular scale. Utilizing host-guest chemistry and coordination-driven self-assembly to construct supramolecular architectures restricts intramolecular rotation and reduces the electrochemical bandgap. Coupled with the catalytic promotion of manganese dioxide nanoflowers, these systems provide exceptional sensitivity for cysteine detection [143].

To further improve electron transfer rates and sensitivity limits, the introduction of biological macromolecular templates has emerged as an efficient strategy. For instance, guiding the ordered assembly of copper NCs via DNA nanobelts (SIEECL) significantly narrows the material bandgap, pushing the detection limit of dopamine to the femtomolar level [144]. Simultaneously, rigid framework

materials are employed to construct intelligent controlled systems that enhance sensing accuracy. Precise energy-level alignment in lanthanide-organic frameworks minimizes energy transfer losses. When coupled with the "redox gate" effect of manganese dioxide nanosheets, this enables ratiometric analysis with an internal reference, substantially improving the reliability of glutathione detection [145]. Furthermore, the rigid confinement of zirconium-based MOFs, combined with aptamer-gated "signal switch" systems, allows for target-triggered quencher release and efficient energy transfer. This provides a highly intelligent response mechanism for adenosine triphosphate (ATP) analysis [146]. Innovation in interfacial reaction mechanisms represents another critical breakthrough. For example, electrochemically generated chlorine microbubbles create a gas/liquid interface that produces a "corona effect". This not only promotes the generation of reactive oxygen species but also extends the reaction zone from the electrode surface into the solution bulk, providing long-lasting signal gain for glucose detection [147]. This ROS-based enhancement strategy can be further advanced by constructing multifunctional enzyme-like composites. These materials directly convert glucose into a co-reactant for *in situ* luminescence, eliminating the dependency on unstable exogenous reagents and enabling the co-detection of alkaline phosphatase [148]. To address the stability challenges of nanoscale materials on electrode surfaces, "atomically precise doping" integrated with "photo-crosslinking" techniques allows for the robust anchoring of luminescent clusters without altering their intrinsic properties. This approach has achieved high-stability glucose sensing on bipolar electrode platforms [108]. Ultimately, these breakthroughs in materials, mechanisms, and interfaces drive the translation of sensing technologies into practical applications. By integrating flexible bipolar electrode arrays, deep eutectic solvent-based solid-state ionogels, and microfluidic patches, fully flexible wearable chip systems have been developed. These systems allow for the *in situ*, real-time monitoring of sweat metabolites, representing a major paradigm shift for ECL technology from laboratory analysis toward home-based health monitoring (Figure 6) [149].

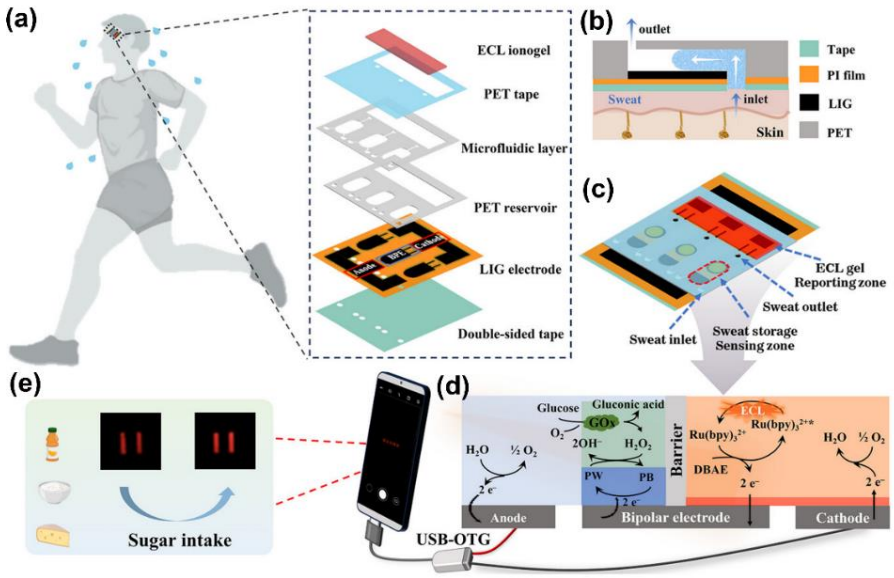

Figure 6. Schematic diagram of the microfluidic flexible ECL array chip for sweat glucose detection. **(a)** Layer assembly of the flexible wearable ECL chip; **(b)** Schematic cross-section of the microfluidic chip for sampling sweat secreted by human sweat glands; **(c)** Schematic of the complete flexible ECL sensing chip; **(d)** Principle of the ECL sensing chip for glucose detection; **(e)** Dual function of smartphone: for ECL chip powering and capturing ECL images. Reprinted with permission [149]. Copyright 2026 Wiley-VCH.

3.4. Ultrasensitive imaging and single-entity analysis

ECL imaging at the single-molecule and single-particle levels represents a paramount challenge in pushing the boundaries of ECL technology. The core difficulty lies in extracting faint optical signals from noisy backgrounds while maintaining high spatiotemporal resolution. This objective requires synergistic innovation across multiple dimensions, including the development of ultra-sensitive photon detection and localization algorithms for absolute quantification, the design of high-performance luminescent nanomaterials for stable signaling, and the exploration of novel modalities such as label-free imaging. Furthermore, the intrinsic spatiotemporal control of ECL can be leveraged to capture transient physicochemical processes. Recently, a series of breakthroughs in these areas has significantly advanced the field [83,150–152].

A milestone achievement in single-molecule ECL detection is the direct imaging and absolute quantification of individual protein molecules. By covalently labeling target proteins with $Ru(bpy)_3^{2+}$ and employing ultra-sensitive single-photon detection systems to capture discrete emission events, researchers have utilized spatiotemporal separation and localization algorithms to achieve precise positioning and counting, pushing detection limits to the attomolar level [153]. Expanding the informational dimensions of imaging is equally vital. For example, co-assembling ligands with distinct luminescent properties to form heterogeneous MOF crystals enables efficient intra-framework energy transfer. This allows for the simultaneous excitation of multi-color ECL at a single-step potential within a single nanoparticle, providing a new platform for multi-color analysis without complex spectral deconvolution [154].

Improving spatial resolution for subcellular imaging is another frontier. Through precise ligand engineering of AuNCs to enhance ECL intensity, researchers have developed ultra-bright, miniaturized probes capable of resolving fine subcellular structures, such as filopodia (~170 nm), demonstrating the immense potential of ECL in cell biology (Figure 7) [81]. In contrast to probe-based “positive contrast” imaging, the label-free “shadow ECL” mode offers unique advantages. This technique relies on the principle that insulating objects on an electrode surface locally obstruct the ECL reaction, creating “shadow” regions. Rigorous optimization of experimental conditions and image processing has improved sensitivity to resolve 100 nm (and even 50 nm) particles, offering a powerful tool for label-free imaging of complex biological samples like microbial spores [155]. ECL imaging also excels at revealing real-time physicochemical dynamics. High-speed ECL microscopy has enabled the *in situ* observation of the “Coulomb explosion” of individual organic microdroplets, providing direct evidence for the behavior of micro-scale fluids under electric fields [156]. Regarding spectral control, integrating molecular crystals as optical waveguides with micro-tubule electrodes has yielded electro-photonic devices capable of active color modulation, such as “blue-to-green” conversion, which paves the way for micro-spectral filters and multi-color sensors [157].

The application of ECL imaging has extended from life sciences to materials science, particularly in characterizing cutting-edge catalysts. A platform for the qualitative and quantitative analysis of trace platinum single-atom catalysts has been developed based on their unique ability to trigger luminol ECL during oxygen reduction, offering new methods for catalyst screening [158]. To optimize enhancement, single-molecule imaging combined with shell-isolated core-shell nanostructures allows for the *in situ* mapping of plasmonic “hotspots”, clarifying the distinct contributions of LSPR and nanoconfinement effects [159]. Exploration of fundamental reaction pathways continues to deepen, such as the discovery

that $Ru(bpy)_3^{2+}$ oxidation in water can be driven by elusive strong reductants, which clarifies water-phase reaction mechanisms [160]. Furthermore, pH-responsive hybrid emitters enable sub-second real-time imaging of local pH gradients during the oxygen evolution reaction (OER), providing critical spatiotemporal data for understanding catalyst degradation [161]. Collectively, these advancements—ranging from single-molecule quantification to multi-color, high-resolution imaging and real-time visualization of interfacial processes—constitute an increasingly sophisticated methodological framework for single-entity ECL analysis.

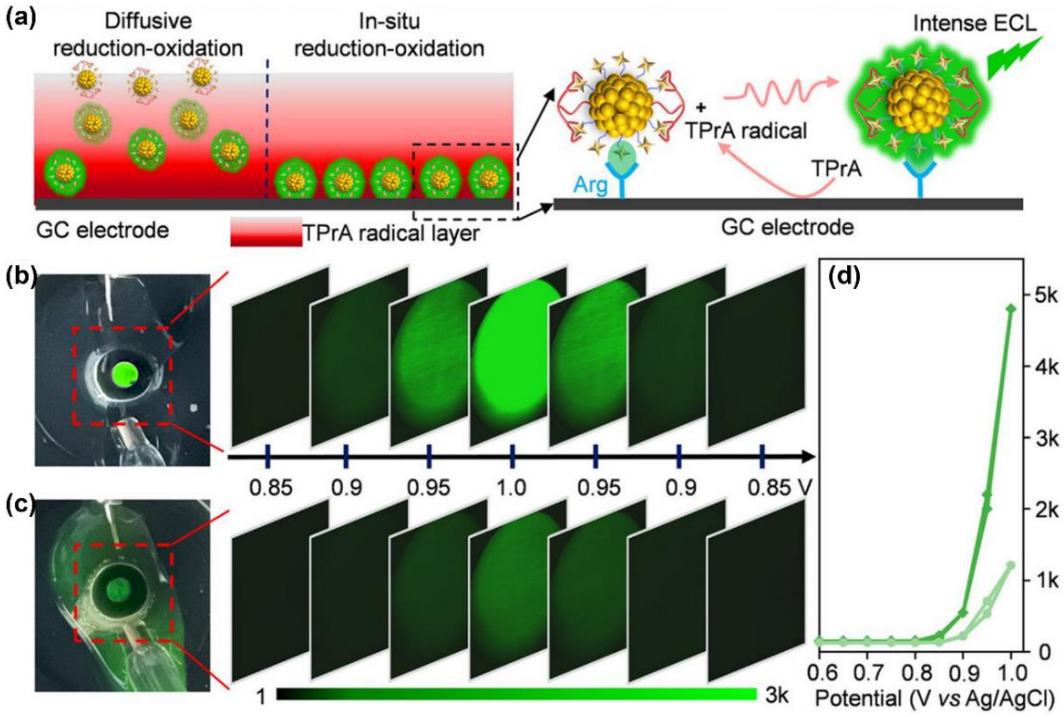

Figure 7. ECL of immobilized CR4/ATT-AuNCs. **(a)** Schematic illustration of the ECL reaction mechanism in diffusive (left) and *in situ* reduction-oxidation pathway (right) of CR4/ATT-AuNCs; **(b)** ECL photograph of *in situ* reduction-oxidation pathway captured by smartphone (left) and corresponding potential-resolved snapshots (right); **(c)** ECL photograph of diffusive reduction-oxidation pathway were captured by smartphone (left) and corresponding potential-resolved snapshots (right); **(d)** ECL traces extracted from b) (green line) and **(c)** (light green line). Reprinted with permission [81]. Copyright 2025 Wiley-VCH.

4. ECL imaging for single-cell analysis

As the fundamental units of life, cells exhibit significant heterogeneity obscured by bulk analysis [162–165]. Single-cell analysis is therefore essential for understanding this complexity and individual cell physiology, offering critical insights for life science and clinical medicine [30,166]. ECL imaging, derived from the convergence of ECL with microscopy, has served as a powerful tool for visualizing cellular functional molecules [23,167]. Featuring near-zero background [168], high sensitivity [169], and excellent spatiotemporal resolution [170], ECL imaging is ideal for long-term dynamic monitoring of living cells. This section highlights key advances in ECL imaging for single-cell detection of cellular secretions, membrane proteins, and intracellular molecules, underscoring the versatility and profound impact of this technology in modern bioscience and nanotechnology.

4.1. ECL imaging of cellular secretions

Cellular secretions, including small molecules, nucleic acids, and proteins, are synthesized by cells and released into the extracellular space, where they play essential roles in intercellular communication, metabolic regulation, and immune defense, thereby maintaining cellular physiology and organismal homeostasis [5,171,172]. Visualizing and interrogating the secretion process at the single-cell level offers a unique window into cellular functional states, responses to stimuli, intercellular communication mechanisms, and adaptation to environmental changes [173,174]. However, most conventional detection methods rely on bulk analysis of secretions collected from large cell populations and thus lack single-cell resolution [175]. This limitation is particularly critical in the tumor microenvironment, where secreted biomolecules diffuse rapidly and secretion profiles vary markedly among individual cells, posing significant challenges for accurate quantification and collection [176,177]. Furthermore, the low concentration and high diffusivity of cellular secretions (e.g., H_2O_2, dopamine) pose significant challenges for real-time *in situ* detection [178,179]. To overcome these challenges, ECL imaging has adopted three main strategies: (i) spatial isolation [180,181], (ii) label-free imaging [182], and (iii) *in situ* co-reactant generation [183]. These approaches have enabled highly sensitive, spatially resolved ECL imaging capable of capturing transient, trace-level secretion events from individual cells.

Trace secreted species (e.g., H_2O_2) generate extremely weak ECL signals, making real-time detection difficult [184]. The "spatial isolation" strategy addresses this limitation by confining molecular transport [185]. This confinement amplifies ECL signals at the secretion site while minimizing interference from the surrounding microenvironment, thereby preserving signal specificity and spatial resolution. Su's group developed a confined ECL platform based on vertically aligned gold microtube electrode ensembles (MEEs) fabricated using a porous polycarbonate membrane template (Figure 8a) [180]. In this system, the tubular architecture spatially confines the ECL reaction and limits the local diffusion of H_2O_2 released from individual cells around each microtube, thereby suppressing signal spreading and crosstalk. As a result, local variations in H_2O_2 concentration are captured as spatially distinct ECL signals, enabling parallel single-cell sensing and revealing heterogeneity in H_2O_2 release at subcellular resolution. By confining analyte diffusion and ECL generation to defined microdomains, this design reduces signal dilution, improves local sensitivity, and enables spatially resolved monitoring of single-cell secretion (Figure 8a).

Based on the concept of spatial confinement, Ju's group developed a confined ECL imaging microarray (CEIM) chip for high-throughput, quantitative analysis of dopamine (DA) release from individual living cells (Figure 8b) [181]. The chip physically isolates single cells within cylindrical microwells, thereby eliminating signal crosstalk. The indium tin oxide (ITO) surface at the base of each microwell was modified with a functional film composed of DA aptamers and co-reactant-embedded polymer dots, enabling *in situ* recognition and strong ECL emission without the addition of an external co-reactant. Captured DA was electrochemically oxidized, which quenched the ECL signal. This enabled highly sensitive quantification of single-cell secretion without external co-reactants. This design addresses the difficulty of collecting highly diffusive secretions and reveals pronounced heterogeneity in hypoxia-induced DA release at the single-cell level.

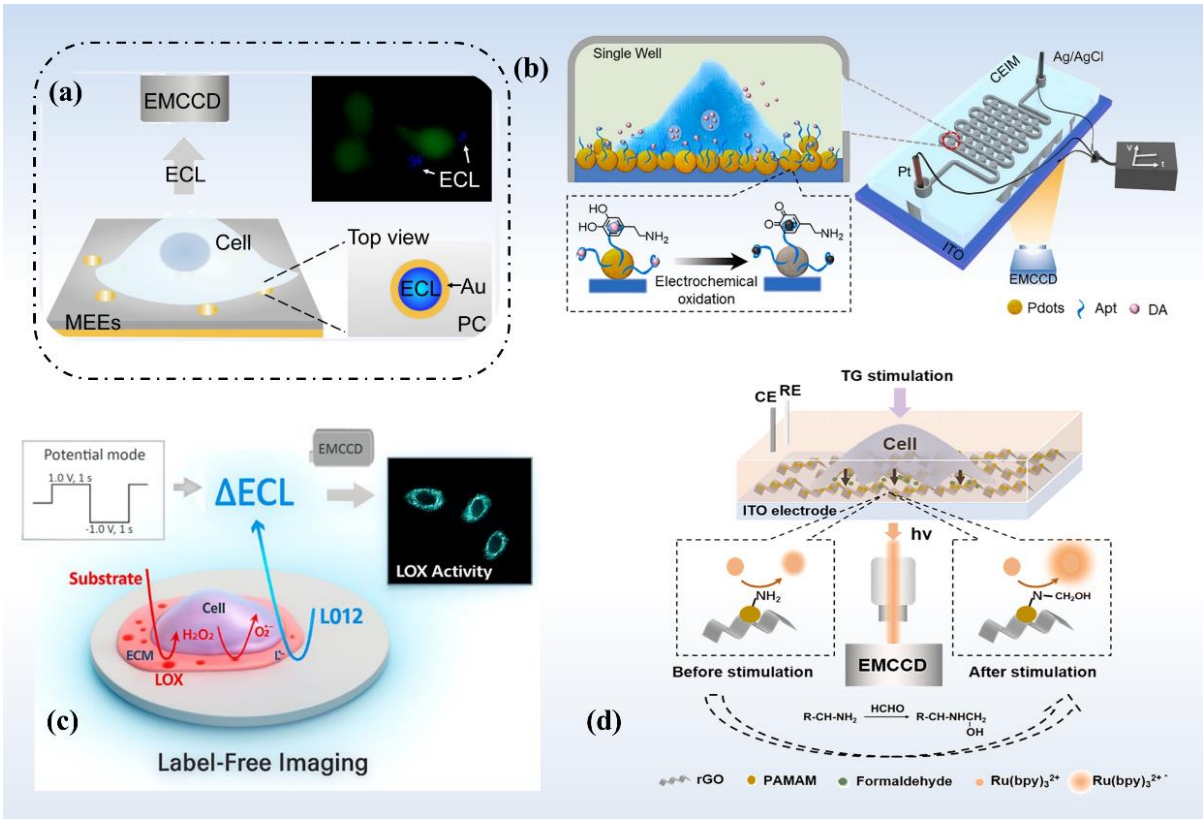

Figure 8. ECL-based detection and imaging of molecular release from single cells. **(a)** Schematic diagram of confined ECL at gold MEEs for the detection of H_2O_2 efflux from single cells. Reprinted with permission [180]. Copyright 2021 WILEY-VCH; **(b)** Schematic diagram of experimental setup of the CEIM chip for detection of DA released from a single cell under hypoxic stimulation. Reprinted with permission [181]. Copyright 2022 Elsevier; **(c)** Schematic diagram of the single-cell enzyme activity imaging system for visualizing secreted LOX activity from single living cells. Reprinted with permission [182]. Copyright 2025 American Chemical Society; **(d)** Schematic diagram of the ECL imaging setup and mechanism of the ECL visualization of FA release from HeLa cells by thapsigargin (TG) stimulation. Reprinted with permission [183]. Copyright 2024 Royal Society of Chemistry.

Label-free imaging directly exploits the intrinsic physical, chemical, or biological properties of target molecules without the need for exogenous labels [186]. By avoiding labelling artefacts, simplifying experimental workflows, and remaining compatible with live-cell and *in vivo* studies, it is increasingly used in single-cell analysis and biomedical imaging. Using this approach, Pan's group developed a label-free ECL microscopy method for imaging lysyl oxidase (LOX) activity in single cells (Figure 8c) [182]. In this system, LOX catalyzes the *in situ* generation of H_2O_2 from L-lysine in the extracellular matrix, and the resulting H_2O_2 acts as a co-reactant for luminol to enhance the ECL signal, thereby enabling spatially resolved imaging of enzyme activity without exogenous labels. Analysis of the ΔECL signal enabled quantification of LOX catalytic efficiency at single-cell resolution, phenotypic classification of enzyme activity (high/low affinity and high/low activity), dynamic monitoring of drug inhibition, and visualization of the spatial heterogeneity of LOX secretion. These measurements further revealed the spatial bias of LOX-mediated extracellular-matrix remodeling during tumor cell migration and extended label-free ECL microscopy to dynamic, high-spatial-resolution analysis of enzyme activity in single cells.

In situ co-reactant generation represents another powerful strategy. It forms co-reactants directly at the electrode surface or reaction interface, thereby avoiding the toxicity associated with externally added co-reactants while simplifying assay design and improving both signal specificity and biocompatibility [187]. This approach is therefore particularly well suited to ECL imaging of living cells at single-cell resolution. Using this principle, Liu's group developed an ECL imaging method for analyzing formaldehyde release from single cells (Figure 8d) [183]. In their design, the terminal amine groups of poly(amidoamine) (PAMAM) dendrimers undergo nucleophilic addition with formaldehyde to generate amino alcohol intermediates *in situ*, which serve as efficient co-reactants for $Ru(bpy)_3^{2+}$. A reduced graphene oxide (rGO)-modified ITO electrode was further introduced to enhance conductivity and electrocatalytic performance. This design eliminates the use of the conventional toxic TPrA co-reactant while enabling a signal-on response, and allows real-time dynamic imaging of formaldehyde released from HeLa cells under TG stimulation. The resulting measurements revealed cell-to-cell heterogeneity in formaldehyde release and illustrated a biocompatible route to sensitive metabolite analysis at the single-cell level.

4.2. ECL imaging of membrane proteins

Cell surface biomolecules are central hubs for cell recognition, signal transduction, and material exchange [188]. Aberrant expression or modification of these species is closely associated with disease mechanisms [189]. For example, heterogeneity in tumor-cell surface markers is a key driver of therapeutic resistance [190]. Specific detection of overexpressed biomolecules on the cell membrane is therefore crucial for early diagnosis and precision therapy [191]. However, existing methods remain limited by insufficient sensitivity and the inability to achieve *in situ* visualization [192]. ECL imaging couples optical spatial resolution with electrochemical spatiotemporal control, offering both high sensitivity and spatial resolution, which makes it well suited for membrane-associated biomolecules [37]. To address the challenges of weak signals and potential cell damage, current studies have developed four main enhancement strategies: (i) self-enhancement (intramolecular electron transfer), (ii) synergistic enhancement (nanostructure-assisted co-reactant loading), (iii) catalytic enhancement (nanozyme-mediated signal amplification), and (iv) physical enhancement (photothermal amplification) [193–196]. In addition, cathodic ECL has emerged as an alternative imaging mode that operates at low potentials and avoids external labels [197].

(1) Self-enhancement. Ju's group developed an ECL microimaging system centered on tertiary amine-conjugated polymer dots (TEA-Pdots) for *in situ*, high-contrast imaging of the membrane protein HER2 on single living cells (Figure 9a) [193]. Two tertiary amine groups were covalently introduced into the poly[(9,9-dioctylfuor-enyl-2,7-diyl)-alt-co-(1,4-benzo-{2,1',3}-thiadiazole)] (PFBT) polymer side chains (TEA-PFBT), enabling markedly enhanced ECL emission at +1.2 V without an added co-reactant. The resulting signal was 132-fold stronger than that obtained from a conventional mixture of Pdots and free TEA (triethylamine), and even surpassed the classical $[Ru(bpy)_3]^{2+}$/TPrA system. This design avoids membrane permeabilization and eliminates the cytotoxicity associated with high concentrations of alkylamines, enabling *in situ*, high-contrast ECL imaging of HER2 on single living cells and dynamic monitoring of siRNA (small interfering RNA)-induced downregulation of protein expression.

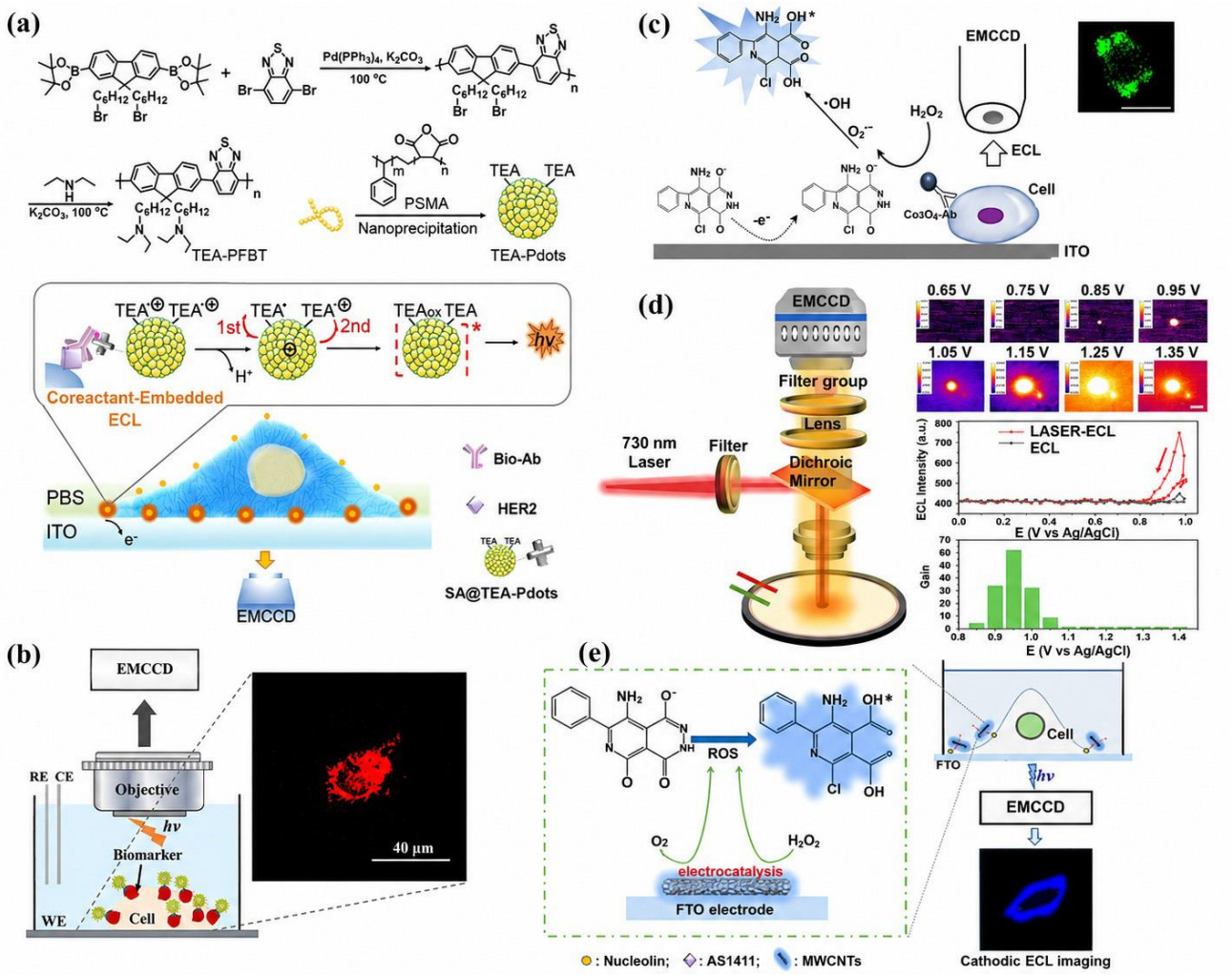

Figure 9. ECL imaging strategies for single-cell membrane analysis. **(a)** (Top) Synthetic route of TEA-PFBT and preparation of TEA-Pdots. (Bottom) Schematic diagram of dual intramolecular electron transfer of TEA-Pdots for ECL microimaging of HER2 on single cells. Reprinted with permission [193]. Copyright 2021 Wiley-VCH; **(b)** Schematic diagram of the ECL imaging of CEA on cell membranes. Reprinted with permission [194]. Copyright 2021 American Chemical Society; **(c)** Schematic diagram of the ECL mechanism based on the Co_3O_4 nanozyme for CEA antigen imaging at the cellular membrane. Reprinted with permission [195]. Copyright 2023 Royal Society of Chemistry; **(d)** Schematic diagram of the HT-ECL device for single cell imaging. Reprinted with permission [196]. Copyright 2023 Royal Society of Chemistry; **(e)** Schematic diagram of cathodic ECL microscopy of MWCNTs for ECL microimaging of nucleolin on a single tumor cell. Reprinted with permission [197]. Copyright 2023 American Chemical Society.

(2) Synergistic enhancement. Jiang's group designed high-index-facet gold nanoflowers (Hi-AuNFs) loaded with guanine-rich single-stranded DNA (G-ssDNA) as synergistic co-reactants for the $Ru(bpy)_3^{2+}$ system (Figure 9b) [194]. Through a catalytic pathway, this design amplified the ECL signal by 234-fold and enabled high-contrast imaging of CEA on the membranes of MCF-7 cells. Owing to their excellent catalytic activity and large specific surface area, Hi-AuNFs serve both as efficient carriers for G-ssDNA and as catalytic amplifiers of the ECL signal. The guanine bases within G-ssDNA act as endogenous co-reactants and further enhance the ECL intensity of $Ru(bpy)_3^{2+}$. By embedding a CEA aptamer within

the G-ssDNA sequence, the probe achieves specific recognition and high-contrast ECL imaging of CEA on the membrane of MCF-7 cells.

(3) Catalytic enhancement. Su's group exploited the peroxidase-like activity of Co_3O_4 nanozymes to construct a catalytically amplified ECL imaging strategy based on the luminol-H_2O_2 system (Figure 9c) [195]. Through Co^{2+}/Co^{3+} redox cycling, the Co_3O_4 nanozyme efficiently catalyzes the decomposition of H_2O_2 into ROS, thereby markedly accelerating the ECL reaction of L012 (a luminol derivative). This increased the ECL intensity by approximately threefold and shortened the imaging exposure time to 500 ms. After conjugation of Co_3O_4 with an anti-CEA antibody, the probe enabled highly sensitive imaging of membrane-associated CEA on MCF-7 cells at a low operating potential of 1.0 V, with a detection limit of 50 pM H_2O_2.

(4) Physical enhancement. Zhu's group developed a heat-triggered ECL (HT-ECL) microscope based on a physical enhancement mechanism (Figure 9d) [196]. Laser irradiation generates micrometer-scale thermal hotspots at the electrode-solution interface, increasing ECL intensity by 63-fold and lowering the onset potential by 0.2 V. This photothermal amplification strategy alleviates membrane damage caused by electrical stimulation and enables high-contrast ECL imaging of membrane proteins on suspended CEM (human acute lymphoblastic leukemia) cells. Compared with conventional ECL imaging methods, this approach improved the imaging contrast by 20.54-fold and shortened the exposure time to 1 s, allowing site-selective analysis of membrane protein abundance at the single-cell level. Point imaging of adherent MCF-7 cells likewise improved the contrast by 4.38-fold. By addressing the challenges of weak signals, high trigger potentials, and the difficulty of imaging suspended cells, this method broadens the scope for sensitive, low-damage visualization of single-cell membrane proteins.

(5) Cathodic ECL as an alternative imaging mode. Zhang's group reported a cathodic ECL microscope based on the luminol analogue L012, enabling label-free imaging of nucleolin on the membranes of single tumor cells (Figure 9e) [197]. In this system, multiwalled carbon nanotubes (MWCNTs) act as efficient co-reactant promoters, catalyzing dissolved oxygen and hydrogen peroxide to generate reactive oxygen species at low trigger potentials, which in turn excite L012 to produce bright cathodic ECL emission. After functionalization of the MWCNT surface with the AS1411 aptamer, the probe specifically recognizes nucleolin overexpressed on tumor-cell membranes, enabling high-contrast imaging of membrane-associated nucleolin at the single-cell level. This cathodic ECL scheme operates at low potential, avoids external labels, and remains biocompatible, making it well suited for low-damage, sensitive analysis of single-cell membrane proteins.

4.3. ECL imaging of intracellular molecules

Intracellular molecular imaging is essential for elucidating subcellular architecture, dynamic molecular transport, and disease-associated signaling [198]. However, exploring the intracellular environment presents unique challenges. Firstly, membrane penetration must be achieved without perturbing the intracellular microenvironment. Secondly, conventional labeling approaches (e.g., fluorescence) and wired detection methods (e.g., nanoelectrodes) are invasive and can interfere with molecular function or damage cells [199,200]. Third, traditional ECL microscopy (ECLM) lacks the sensitivity required for imaging at physiological concentrations. To overcome these limitations, recent work has developed three classes of ECL strategies for intracellular analysis: (i) stimulus-responsive dynamic imaging [201], (ii) wireless low-damage electroanalysis [202], and (iii) label-free high-sensitivity imaging [203,204].

(1) Stimulus-responsive dynamic imaging. Liu's group developed a stimulus-responsive self-assembled DNA nanomachine for ECL imaging of intracellular ATP in single cells (Figure 10a) [201]. The probe uses $Ru(bpy)_3^{2+}$-doped metal-organic frameworks (RuMOFs) as the core luminophore and is coated with a DNA polymer hydrogel (DNAgel) containing ATP aptamers, which blocks electron transfer from the co-reactant and thereby quenches the ECL signal. After cellular uptake, intracellular ATP specifically binds the aptamer, which triggers dissociation of the DNAgel, thereby exposing the RuMOF and restoring ECL emission. This nanomachine enabled three-dimensional imaging of the spatial distribution of ATP in MCF-7 cells (z = 0, 0.5 and 1 μm) and discriminated ATP levels between cancer cells (MCF-7 and HeLa) and normal cells (MCF-10A).

(2) Wireless low-damage electroanalysis. To address the need for direct cell-electrode contact in conventional ECL imaging, which has hindered wireless detection of intracellular proteins, Chen's group developed a wireless imaging strategy based on bipolar ECL (BPE-ECL) for intracellular antigen imaging in individual cells (Figure 10b) [202]. Single-walled carbon nanotubes (SWCNTs) were conjugated with antibodies against KDM1/LSD1 (lysine-specific demethylase 1, also known as KDM1) and introduced into MCF-7 cells by endocytosis to specifically target the antigen within the nucleus. After the cells were embedded in agarose hydrogel and exposed to an electric field of 1 kV/cm, the SWCNTs acted as bipolar electrodes: dissolved oxygen was reduced at the cathodic pole, whereas L012 was oxidized at the anodic pole to generate ECL emission. The spatial confinement imposed by the hydrogel micropores lowered the required field strength by an order of magnitude and effectively avoided cell damage. This study represents the first wireless ECL imaging of intracellular proteins.

(3) Label-free high-sensitivity imaging. Zhu's group devised a bio-coreactant-enhanced ECL microscopy technique using endogenous co-reactants for label-free, highly sensitive imaging of intracellular structures and dynamic molecular transport (Figure 10c) [203]. In this strategy, $Ru(bpy)_3^{2+}$ serves as an electrochemical molecular antenna: after oxidation at the electrode surface to $Ru(bpy)_3^{3+}$, it forms a diffusion layer that spans the entire cell. Once inside the cell, $Ru(bpy)_3^{3+}$ undergoes catalytic ECL reactions with endogenous amine-rich biomolecules such as DNA, RNA, and histones, without the need for exogenous co-reactants or labels. This method successfully imaged subcellular structures in HeLa cells, including nucleoli, the nucleus, and the endoplasmic reticulum. Time-resolved ECL further revealed heterogeneous transport of $Ru(bpy)_3^{3+}$ from the cell periphery to the nuclear region, with transport velocity negatively correlated with actin cytoskeleton density. In addition, Sojic's group developed a shadow ECL (SECL) microscope based on physical obstruction for label-free, highly sensitive imaging of individual mitochondria deposited on an electrode surface (Figure 10d) [204]. This system uses the direct-oxidation ECL pathway of $Ru(bpy)_3^{2+}$ and TPrA, confining the emitting layer to a micrometer-scale thickness at the electrode surface. Deposited mitochondria physically obstruct the diffusion of ECL reagents and therefore appear as high-contrast dark spots in the ECL image, yielding negative contrast. Co-localization with fluorescence labels confirmed the specificity of SECL. Statistical analysis showed that SECL could detect small mitochondria with areas below 0.5 μm^2, which were difficult to resolve by fluorescence methods. Moreover, the exposure time required for SECL (0.2 s) was far shorter than that for fluorescence imaging (5 s), and no photobleaching or phototoxicity was observed.

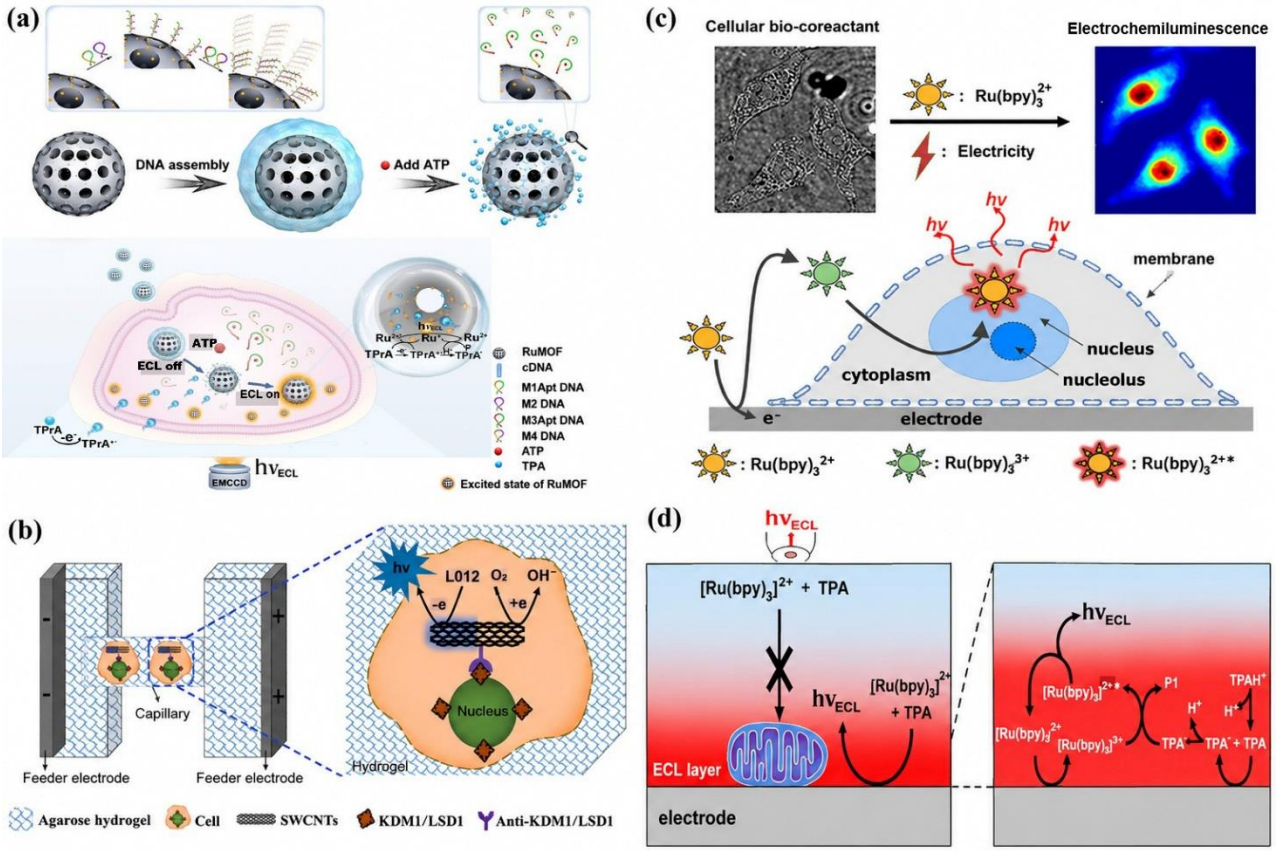

Figure 10. ECL imaging strategies for intracellular structures and subcellular analysis. **(a)** Schematic diagram of the preparation of the stimuli-responsive self-assembled DNA nanomachine and the intracellular ATP-triggered ECL visualization. Reprinted with permission [201]. Copyright 2024 Wiley-VCH; **(b)** Schematic diagram of the BPE-ECL wireless setup for electrochemical visualization of KDM1/LSD1 antigen in the cell nucleus. Reprinted with permission [202]. Copyright 2022 CCS Chemistry; **(c)** Schematic diagram of the bio-coreactant-enhanced ECL microscopy of intracellular structure and transport, using the guanine moiety of nucleic acid as an example of a bio-coreactant in the "catalytic route" of $Ru(bpy)_3^{2+}$ ECL reactions. Reprinted with permission [203]. Copyright 2021 Wiley-VCH; **(d)** Schematic diagram of label-free shadow ECL microscopy (SECL) of single mitochondria. Left: side-view scheme based on spatial confinement of the ECL-emitting layer. Right: the direct oxidation ECL mechanism of $Ru(bpy)_3^{2+}$ and TPA, which restricts the spatial extension of the light-emitting layer. Reprinted with permission [204]. Copyright 2021 Wiley-VCH.

Despite encouraging progress in ECL imaging of single-cell secretions, membrane proteins, and intracellular molecules, two technical challenges remain. Firstly, multiplexed imaging remains limited. Most current ECL strategies focus on a single target, and cannot yet provide synchronous, dynamic analysis of multiple intracellular events and their interactions. Secondly, long-term dynamic observation of living cells is still difficult. During extended imaging, issues such as probe stability, cell viability, and interfacial biocompatibility remain unresolved, constraining the complete capture of dynamic cellular processes.

5. Prospects and outlooks

ECL biosensing has established itself as a pivotal bridge linking advanced functional materials, precision interfacial engineering, and the decoding of complex biological information. This field has demonstrated remarkable methodological vitality and broad application prospects, ranging from the rational design of high-performance luminophores—such as MOFs, COFs, perovskites, and AIE materials—to highly sensitive and selective detection strategies for diverse biomarkers including proteins, nucleic acids, and small molecules. Furthermore, single-molecule and single-particle imaging, alongside real-time dynamic analysis, continue to push the boundaries of sensitivity to their physical limits. Looking ahead, the advancement of ECL technology toward deeper life science explorations and broader point-of-care testing (POCT) requires breakthroughs across several critical dimensions. The development of novel ECL luminophores that combine ultra-high brightness, excellent biocompatibility, and long-wavelength (near-infrared/infrared) emission is fundamental for driving real-time *in vivo* imaging and deep-tissue analysis. Additionally, the promotion of fully integrated, miniaturized, and intelligent sensing systems is essential. This involves the seamless integration of sample preprocessing, target enrichment, signal generation, and readout modules onto Lab-on-a-Chip platforms. Incorporating machine learning algorithms for automated data analysis and diagnosis will truly address the requirements of bedside diagnostics and home health monitoring. In addition, deepening the understanding of fundamental ECL physicochemical processes—particularly charge transfer, energy migration, and reaction kinetics at the single-entity level—will provide the essential theoretical guidance to design next-generation, disruptive ECL materials and sensing paradigms. It is foreseeable that the profound integration of materials science, micro-nanofabrication, data science, and biomedicine will position ECL biosensing as a core technology in precision medicine, environmental monitoring, and biosafety. This evolution will ultimately facilitate a paradigm shift from high-sensitivity detection to intelligent, dynamic perception.

Although ECL imaging has achieved some progress in the analysis of single-cell secretions, membrane proteins, and intracellular molecules, exploring deeper questions in life science requires to overcome several technical bottlenecks and establish new research paradigms. Achieving synchronous multi-target imaging is a critical step toward understanding complex cellular functional networks. Most current ECL strategies focus on a single analyte, which limits the ability to simultaneously reveal interactions within multiple signaling pathways. Future developments should prioritize multiplexed ECL imaging probes based on potential resolution, wavelength resolution, or lifetime resolution. These probes, combined with microarray electrodes and algorithmic decoupling, will enable the dynamic, *in-situ* parallel monitoring of various biomolecules—such as cytokines, membrane receptor clusters, and metabolites—at the single-cell level. Furthermore, enhancing spatiotemporal resolution and achieving long-term, non-destructive observation are essential for unlocking dynamic life processes. The development of brighter and more photostable near-infrared or infrared ECL emitters is necessary. Integrating these emitters with super-resolution techniques, such as those based on local reaction confinement or plasmonic enhancement, can push spatial resolution to the sub-organelle or even nanometer scale. This allows for millisecond-level tracking of rapid processes, including vesicle trafficking and protein aggregate formation. Meanwhile, the development of biocompatible interface materials, self-powered sensing systems utilizing endogenous substances, and low-potential or wireless excitation modes is vital to maintaining cell viability during long-term kinetic studies spanning hours or days. A deeper

integration of ECL technology with biological research is required to expand its application boundaries. This includes coupling ECL imaging with omics technologies, such as single-cell sequencing and mass spectrometry, to correlate high-resolution molecular distributions with cellular genotypes and global molecular phenotypes. The development of miniaturized and implantable ECL imaging devices is also crucial for the *in vivo*, real-time monitoring of tumor microenvironments, neurotransmitter release, or immune cell activities. Moreover, leveraging the high-throughput and high-sensitivity advantages of ECL imaging can facilitate frontier applications in precision medicine, such as organoid screening and drug efficacy or toxicity evaluation. It is foreseeable that, through continued interdisciplinary convergence, ECL single-cell imaging will evolve from a powerful analytical tool into an indispensable platform for systematically decoding the spatiotemporal logic of life at single-cell precision.

Declaration of generative AI and AI-assisted technologies

During the preparation of this manuscript, the authors used generative AI tools only to improve language and readability. Specifically, the authors used Doubao, Yuanbao, Deepseek, and ChatGPT for language polishing in entire manuscript. The authors take full responsibility for the content of the manuscript.

Acknowledgments

This work was financially supported by the National Natural Science Foundation of China (21827812, 21890741).

Authors' contribution

Conceptualization, Lele Li and Xue Dong; writing—original draft preparation, Lele Li and Xue Dong; supervision, Qin Wei and Huangxian Ju; writing—review and editing, Huangxian Ju; funding acquisition, Huangxian Ju. All authors have read and agreed to the published version of the manuscript.

Conflicts of interest

Huangxian Ju holds the position of Editor-in-Chief for *Life Analysis* and has not peer reviewed or made any editorial decisions for this paper.

References

[1] Cui H, Paolucci F, Sojic N, Xu G. Analytical electrochemiluminescence. *Anal. Bioanal. Chem.* 2016, 408(25):7001–7002.

[2] Hu L, Xu G. Applications and trends in electrochemiluminescence. *Chem. Soc. Rev.* 2010, 39(8):3275–3304.

[3] Khonsari, YN, Sun S. Recent trends in electrochemiluminescence aptasensors and their applications. *Chem. Commun.* 2017, 53(65):9042–9054.

[4] Wang H. Advances in electrochemiluminescence co-reaction accelerator and its analytical applications. *Anal. Bioanal. Chem.* 2021, 413(16):4119–4135.

[5] Ma C, Cao Y, Gou X, Zhu J. Recent progress in electrochemiluminescence sensing and imaging. *Anal. Chem.* 2019, 92(1):431–454.

[6] Yan Y, Ding L, Ding J, Zhou P, Su B. Recent advances in electrochemiluminescence visual biosensing and bioimaging. *ChemBioChem* 2024, 25(23):e202400389.

[7] Valenti G, Fiorani A, Li H, Sojic N, Paolucci F. Essential role of electrode materials in electrochemiluminescence applications. *ChemElectroChem* 2016, 3(12):1990–1997.

[8] Czioska S, Chen Z. Electrogenerated chemiluminescence of the tris(2,2′-bipyridine)ruthenium(ii)/aliphatic amine system: a universal effect of perchlorate salts. *RSC Adv.* 2016, 6(8):6583–6588.

[9] Ding Z, Quinn BM, Haram SK, Pell LE, Korgel BA, *et al.* Electrochemistry and electrogenerated chemiluminescence from silicon nanocrystal quantum dots. *Science* 2002, 296(5571):1293–1297.

[10] Hesari M, Ding Z. Efficient near-infrared electrochemiluminescence from Au_{18} nanoclusters. *Chem. Eur. J.* 2021, 27(60):14821–14825.

[11] Wang Y, Zhao G, Chi H, Yang S, Niu Q, *et al.* Self-luminescent lanthanide metal–organic frameworks as signal probes in electrochemiluminescence immunoassay. *J. Am. Chem. Soc.* 2020, 143(1):504–512.

[12] Xu Y, Liu J, Gao C, Wang E. Applications of carbon quantum dots in electrochemiluminescence: A mini review. *Electrochem. Commun.* 2014, 48:151–154.

[13] Feng Y, Wang N, Ju H. Highly efficient electrochemiluminescence of cyanovinylene-contained polymer dots in aqueous medium and its application in imaging analysis. *Anal. Chem.* 2017, 90(2):1202–1208.

[14] Chen Y, Zhou S, Li L, Zhu J. Nanomaterials-based sensitive electrochemiluminescence biosensing. *Nano Today* 2017, 12:98–115.

[15] Nikolaou P, Valenti G, Paolucci F. Nano-structured materials for the electrochemiluminescence signal enhancement. *Electrochim. Acta* 2021, 388:138586.

[16] Han D, Vidic J, Jiang D, Loget G, Sojic N. Photoinduced electrochemiluminescence immunoassays. *Anal. Chem.* 2024, 96(45):18262–18268.

[17] Hu X, Jia X, Zhang K, Lo TW, Fan Y, *et al.* Deep-learning-augmented microscopy for super-resolution imaging of nanoparticles. *Opt. Express* 2023, 32(1):879–890.

[18] Zhang J, Arbault S, Sojic N, Jiang D. Electrochemiluminescence imaging for bioanalysis. *Annu. Rev. Anal. Chem.* 2019, 12(1):275–295.

[19] Wang H, Yuan Y, Chai Y, Yuan R. Self-enhanced electrochemiluminescence immunosensor based on nanowires obtained by a green approach. *Biosens. Bioelectron.* 2015, 68:72–77.

[20] Meng X, Pang X, Yang J, Zhang X, Dong H. Recent advances in electrochemiluminescence biosensors for microrna detection. *Small* 2024, 20(22):2307701.

[21] Valenti G, Scarabino S, Goudeau B, Lesch A, Jović M, *et al.* Single cell electrochemiluminescence imaging: from the proof-of-concept to disposable device-based analysis. *J. Am. Chem. Soc.* 2017, 139(46):16830–16837.

[22] Zanut A, Fiorani A, Canola S, Saito T, Ziebart N, *et al.* Insights into the mechanism of coreactant electrochemiluminescence facilitating enhanced bioanalytical performance. *Nat. Commun.* 2020, 11(1):2668.

[23] Dong J, Feng J. Electrochemiluminescence from single molecule to imaging. *Anal. Chem.* 2023, 95(1):374–387.

[24] Liu Y, Zhang H, Li B, Liu J, Jiang D, *et al.* Single biomolecule imaging by electrochemiluminescence. *J. Am. Chem. Soc.* 2021, 143(43):17910–17914.

[25] Ding H, Guo W, Su B. Imaging cell-matrix adhesions and collective migration of living cells by electrochemiluminescence microscopy. *Angew. Chem. Int. Edit.* 2020, 59(1):449–456.
[26] Ding L, Ding H, Zhou P, Xi L, Su B. Surface-sensitive imaging analysis of cell–microenvironment interactions by electrochemiluminescence microscopy. *Anal. Chem.* 2022, 94(30):10885–10892.
[27] Zhou Y, Dong J, Zhao P, Zhang J, Zheng M, *et al.* Imaging of single bacteria with electrochemiluminescence microscopy. *J. Am. Chem. Soc.* 2023, 145(16):8947–8953.
[28] Deng Y, He X, Jin R, Jiang D, Fang D. Local electrochemiluminescence imaging using scanning electrochemical cell microscopy. *Electrochem. Commun.* 2024, 164:107737.
[29] Huang C, Liu Z, Xu J, Li L, Chen Y, *et al.* Label-free evanescent imaging of cellular heterogeneity in membrane protein binding kinetics. *Sensor. Actuat. B-Chem.* 2024, 419:136377.
[30] He Q, Ma Z, Yang Y, Xu C, Zhao W. Recent advances in electrochemiluminescence-based single-cell analysis. *Chemosensors* 2023, 11(5):281.
[31] Ding H, Guo W, Zhou P, Su B. Nanocage-confined electrochemiluminescence for the detection of dopamine released from living cells. *Chem. Commun.* 2020, 56(59):8249–8252.
[32] Gao W, Liu Y, Zhang H, Wang Z. Electrochemiluminescence biosensor for nucleolin imaging in a single tumor cell combined with synergetic therapy of tumor. *ACS Sens.* 2020, 5(4):1216–1222.
[33] Xu J, Huang P, Qin Y, Jiang D, Chen H. Analysis of intracellular glucose at single cells using electrochemiluminescence imaging. *Anal. Chem.* 2016, 88(9):4609–4612.
[34] Cheow LF, Courtois ET, Tan Y, Viswanathan R, Xing Q, *et al.* Single-cell multimodal profiling reveals cellular epigenetic heterogeneity. *Nat. Methods* 2016, 13(10):833–836.
[35] Chen J. Perspectives on somatic reprogramming: spotlighting epigenetic regulation and cellular heterogeneity. *Curr. Opin. Genet. Dev.* 2020, 64:21–25.
[36] Zhou J, Zhang S, Liu Y. Electrochemiluminescence single-cell analysis on nanostructured interface. *Electroanal.* 2022, 34(6):937–946.
[37] Wang C, Liu S, Ju H. Electrochemiluminescence nanoemitters for immunoassay of protein biomarkers. *Bioelectrochemistry* 2023, 149:108281.
[38] Deng M, Zhong M, Li M, Huang G, He H, *et al.* Research progress on electrochemiluminescence nanomaterials and their applications in biosensors—a review. *Anal. Chim. Acta* 2025, 1361:344148.
[39] Muzyka K. Current trends in the development of the electrochemiluminescent immunosensors. *Biosens. Bioelectron.* 2014, 54:393–407.
[40] Horiuchi T, Niwa O, Hatakenaka N. Evidence for laser action driven by electrochemiluminescence. *Nature* 1998, 394:659–661.
[41] Wang H, Chai Y, Li H, Yuan R. Sensitive electrochemiluminescent immunosensor for diabetic nephropathy analysis based on tris(bipyridine) ruthenium(ii) derivative with binary intramolecular self-catalyzed property. *Biosens. Bioelectron.* 2018, 100:35–40.
[42] Cui H, Zou G, Lin X. Electrochemiluminescence of luminol in alkaline solution at a paraffin-impregnated graphite electrode. *Anal. Chem.* 2003, 75(2):324–331.
[43] Forster RJ, Bertoncello P, Keyes TE. Electrogenerated chemiluminescence. *Annu. Rev. Anal. Chem.* 2009, 2(1):359–385.
[44] Tokel NE, Bard AJ. Electrogenerated chemiluminescence. IX. Electrochemistry and emission from systems containing tris(2,2'-bipyridine)ruthenium(ii) dichloride. *J. Am. Chem. Soc.* 1972, 94(8):2862–2863.

[45] Miao W, Choi J, Bard AJ. Electrogenerated chemiluminescence 69: The Tris(2,2′-bipyridine)ruthenium(ii), ($Ru(bpy)_3^{2+}$)/Tri-n-propylamine (TPrA) system revisiteds-a new route involving $TPrA^{\bullet+}$ cation radicals. *J. Am. Chem. Soc.* 2002, 124(48):14478–14485.

[46] Shen L, Li X, Qi H, Zhang C. Electrogenerated chemiluminescence of ruthenium complex immobilized in a highly cross-linked polymer and its analytical applications. *Luminescence* 2008, 23(6):370–375.

[47] Deiss F, LaFratta CN, Symer M, Blicharz TM, Sojic N, *et al.* Multiplexed sandwich immunoassays using electrochemiluminescence imaging resolved at the single bead level. *J. Am. Chem. Soc.* 2009, 131(17):6088–6089.

[48] Dang J, Guo Z, Zheng X. Label-free sensitive electrogenerated chemiluminescence aptasensing based on chitosan/$Ru(bpy)_3^{2+}$/silica nanoparticles modified electrode. *Anal. Chem.* 2014, 86(18):8943–8950.

[49] Hailaxi A, Cheng G, Chai R, Song Y, Shen Z, *et al.* Novel label-free electrochemiluminescence immunosensor based on Ru@SiO_2-PEI-Au@Pt hybrid nanostructures for highly sensitive PSA detection. *Electroanalysis* 2026, 38(2):e70101.

[50] Kala AB, Rajeevan G, Madanan AS, Varghese S, Abraham MK, *et al.* Immunosensing of cardiac troponin I (cTnI) using a two-electrode electrochemiluminescence platform with near persisting luminescence generated on a $Ru(bpy)_3^{2+}$-tripropylamine system. *ACS Appl. Bio Mater.* 2024, 7(11):7700–7709.

[51] Haghighatbin MA, Laird SE, Hogan CF. Electrochemiluminescence of cyclometalated iridium (III) complexes. *Curr. Opin. Electrochem.* 2018, 7:216–223.

[52] Guan R, Xie L, Ji L, Chao H. Phosphorescent iridium(III) complexes for anticancer applications. *Eur. J. Inorg. Chem.* 2020, 2020(42):3978–3986.

[53] Zhao K, Shan G, Fu Q, Su Z. Tuning emission of AIE-active organometallic Ir(III) complexes by simple modulation of strength of donor/acceptor on ancillary ligands. *Organometallics* 2016, 35(23):3996–4001.

[54] Guo W, Ding H, Gu C, Liu Y, Jiang X, *et al.* Potential-resolved multicolor electrochemiluminescence for multiplex immunoassay in a single sample. *J. Am. Chem. Soc.* 2018, 140(46):15904–15915.

[55] Ouyang C, Wang C. Electrochemical characterization of the clay-enhanced luminol ECL reaction. *J. Electroanal. Chem.* 1999, 474(1):82–88.

[56] Wang W, Cui H, Deng Z, Dong Y, Guo J. A general E-E/C mechanism for the counter-peak in luminol electrochemiluminescence. *J. Electroanal. Chem.* 2008, 612(2):277–287.

[57] Knight AW. A review of recent trends in analytical applications of electrogenerated chemiluminescence. *TrAC Trends Anal. Chem.* 1999, 18:47–62.

[58] Liu S, Yuan H, Bai H, Zhang P, Lv F, *et al.* Electrochemiluminescence for electric-driven antibacterial therapeutics. *J. Am. Chem. Soc.* 2018, 140(6):2284–2291.

[59] Jiang X, Wang H, Wang H, Zhuo Y, Yuan R, *et al.* Self-enhanced N-(aminobutyl)-N-(ethylisoluminol) derivative-based electrochemiluminescence immunosensor for sensitive laminin detection using PdIr cubes as a mimic peroxidase. *Nanoscale* 2016, 8(15):8017–8023.

[60] Ma S, Sun H, Li Y, Qi H, Zheng J. Discrimination between 5-hydroxymethylcytosine and 5-methylcytosine in DNA via selective electrogenerated chemiluminescence (ECL) labeling. *Anal. Chem.* 2016, 88(20):9934–9940.

[61] Yang H, Wang H, Xiong C, Chai Y, Yuan R. Intramolecular self-enhanced nanochains functionalized by an electrochemiluminescence reagent and its immunosensing application for the detection of urinary β2-microglobulin. *ACS Appl. Mater. Interfaces* 2017, 9(41):36239–36246.

[62] Marquette CA, Leca BD, Blum LJ. Electrogenerated chemiluminescence of luminol for oxidase-based fibre-optic biosensors. *Luminescence* 2001, 16(2):159–165.

[63] Tokel NE, Keszthelyi CP, Bard AJ. Electrogeneratedchemiluminescence. X. .alpha.,.beta.,.gamma.,.delta.-tetraphenylporphin chemiluminescence. *J. Am. Chem. Soc.* 1972, 94(14):4872–4877.

[64] Ishimatsu R, Takano E. Intense annihilation electrogenerated chemiluminescence from tris(2-phenylpyridinato)iridium(III) with organic radical cations and anions. *J. Electroanal. Chem.* 2024, 971:118589.

[65] Slaterbeck AF, Meehan TD, Gross EM, Wightman RM. Selective population of excited states during electrogenerated chemiluminescence with 10-methylphenothiazine. *J. Phys. Chem. B* 2002, 106(23):6088–6095.

[66] Attanayake NH, Kowalski JA, Greco KV, Casselman MD, Milshtein JD, *et al.* Tailoring two-electron-donating phenothiazines to enable high-concentration redox electrolytes for use in nonaqueous redox flow batteries. *Chem. Mater.* 2019, 31(12):4353–4363.

[67] Pal P, Paul B, Datta A, Malik S. Aryl-substituted buta-1,3-diene and phenothiazine based solid-state emissive copolymers: photophysical properties and electrochromic behaviors. *ACS Appl. Polym. Mater.* 2024, 6(17):10882–10890.

[68] Zhao Y, Bouffier L, Xu G, Loget G, Sojic N. Electrochemiluminescence with semiconductor (nano)materials. *Chem. Sci.* 2022, 13(9):2528–2550.

[69] Zhong C, Zhang X, Gong Z, Xu H. Recent advances in electroluminescent metallic nanoclusters: From materials to devices. *Nano Lett.* 2024, 24(31):9415–9428.

[70] Li H, Tian L, Yang S, Li C, Li R, *et al.* Solid-state electrochemiluminescence sensor based on TiO_2@CdSe and $Ru(bpy)_3^{2+}$@Ag NPs for ultrasensitive detection of malathion. *Food Chem.* 2025, 470:142726.

[71] Lai Q, Xu J, Fang X, Pan J, Song X, *et al.* Dual enhancement of electrochemiluminescence imaging for single Au-mSiO_2-CdSe nanoparticles via resonance energy transfer and interlayer conductivity. *Anal. Chem.* 2025, 97(12):6796–6803.

[72] Liu J, Yang Y, Jin Y, Zhou Y, Shen Z, *et al.* Silver doping-induced electrochemiluminescence enhancement of cdte quantum dots combined with hairpin-fueled entropy-driven reactions strategy for ultrasensitive bioanalysis. *Biosens. Bioelectron.* 2025, 286:117555.

[73] Gu C, Ji S, Chen Z, Yang W, Deng Y, *et al.* Enrichment-catalytic synergistically enhanced electrochemiluminescence sensors based on IrMOF-3/CdTe for ultrasensitive detection of organophosphorus pesticides. *Biosens. Bioelectron.* 2025, 279:117398.

[74] Huang Z, Wang M, Li H, Wang S, Song X, *et al.* Controlled release competitive electrochemiluminescence sensor based on PbS QDs as novel quencher for ultrasensitive monitoring of environmental pollutant. *Chem. Eng. J.* 2025, 518:164574.

[75] Dong S, Gao X, Fu L, Jia J, Zou G. Low-triggering-potential electrochemiluminescence from surface-confined $CuInS_2$@ZnS nanocrystals and their biosensing applications. *Anal. Chem.* 2021, 93(36):12250–12256.

[76] Yang Y, Guo Y, Shen Z, Liu J, Yuan R, *et al.* Agaus quantum dots as a highly efficient near-infrared electrochemiluminescence emitter for the ultrasensitive detection of microrna. *Anal. Chem.* 2023, 95(24):9314–9322.

[77] Li M, Gao X, Ren X, Ai Y, Zhang B, *et al.* Potential-selective electrochemiluminescence of $AgInS_2$/ZnS nanocrystals and its immunoassay application. *Chem. Commun.* 2024, 60(37):4958–4961.

[78] Wang Z, Liu K, Li F, Li H, Wang W, *et al.* Long-term stable electrochemiluminescence of perovskite quantum dots in aqueous media. *Chem. Commun.* 2024, 60:10962–10965.

[79] Huang Y, Feng Y, Li F, Lin F, Wang Y, *et al.* Sensing studies and applications based on metal halide perovskite materials: Current advances and future perspectives. *TrAC Trends Anal. Chem.* 2021, 134:116127.

[80] Li J, Wu Z, Luo F, Lin Z, Wang J, *et al.* Stable halide perovskite $CsPbBr_3$ nanocrystals assisted by covalent-organic frameworks for electrochemiluminescence analysis in an aqueous medium. *Anal. Chem.* 2024, 96(42):16783–16792.

[81] Zhou K, Tang Z, Liu Y, Xing Z, Zhu J, *et al.* Ultrabright gold nanoclusters with intra-cluster hydrogen bonding enable near-zero-thickness electrochemiluminescence imaging of subcellular structures. *Angew. Chem. Int. Edit.* 2025, 137(52):e10193.

[82] Ge J, Zhang H, Chen X, Song H, Zhou T, *et al.* Cation-induced assembly confers aqueous stability on magic-sized clusters for enhanced electrochemiluminescence. *Anal. Chem.* 2026, 98(2):1617–1627.

[83] Chen J, Jia Y, Zhao H, Wu D, Du Y, *et al.* Ternary heterojunction ZnS-$ZnIn_2S_4$-In_2S_3 efficiently catalyzes triethylamine to enhance electrochemiluminescence imaging signals. *Adv. Funct. Mater.* 2025, 35(17):2420714.

[84] Zhen M, Wang Y, Xu C, Yi Y, Huang J, *et al.* Dual-enhanced electrochemiluminescence of au nanoclusters: Ag doping-induced emission and Ce-MOFs-induced excitation. *Biosens. Bioelectron.* 2025, 288:117833.

[85] Jia D, Zhang X, Jia Y, Liu X, Du Y, *et al.* Mesostructured silica xerogel-encapsulated gold nanoclusters as an electrochemiluminescence emitter combined with a DNA walker amplification strategy for detection of Ochratoxin A. *Anal. Chem.* 2025, 97(12):6464–6472.

[86] Su J, Xiang D, Zhong W, Fu Y, Diao R, *et al.* Electrochemiluminescence monitoring of the ligand exchange process of gold nanoclusters. *Anal. Chem.* 2025, 97:22797–22806.

[87] Huang Y, Hu X, Zhang W, Zheng J, Shao J, *et al.* Multiwalled carbon nanorings found in raw single-walled carbon nanotubes and applied for electrochemiluminescent immunoassay. *ACS Sens.* 2025, 10(6):4589–4599.

[88] Wang H, Liu P, Peng J, Yu H, Wang L. Poly(3,4-ethylenedioxythiophene):Poly(styrene sulfonate) modified metal-organic frameworks boosting carbon dots electrochemiluminescence emission for sensitive miRNA detection. *Biosens. Bioelectron.* 2024, 249:116015.

[89] Wei X, Su Y, Jiang M, Ji H, Zhang R, *et al.* Ultra-sensitive detection of Cu^{2+} in water and infant formula using a carbon dot-embedded MIL-53 electrochemiluminescence sensor. *Food Chem.* 2025, 485:144338.

[90] He Y, Zhang X, Shi L, Zeng B. Preparation of a low-toxic biomass-derived carbon dots-based magnetic molecular imprinting electrochemiluminescence sensor for the rapid separation and highly sensitive detection of zearalenone. *Food Chem.* 2025, 499:147330.

[91] Mei X, Zhou S, Zhang J, Yan M, Yu J, *et al.* Self-releasing reactive oxygen species based on the metal-to-MOF charge transfer effect boost electrochemiluminescence. *Chem. Sci.* 2026, 17(11):5585–5594.

[92] Yu D, Zhang H, Ren J, Qu X. Hydrogen-bonded organic frameworks: new horizons in biomedical applications. *Chem. Soc. Rev.* 2023, 52(21):7504–7523.

[93] Cao Y, Wu R, Gao Y, Zhou Y, Zhu J. Advances of electrochemical and electrochemiluminescent sensors based on covalent organic frameworks. *Nano-Micro Lett.* 2024, 16(1):37.

[94] Wang X, Wan R, Tang Y, Sun S, Chen H, *et al.* Aggregation-induced emission materials-based electrochemiluminescence emitters for sensing applications: progress, challenges and perspectives. *Coord. Chem. Rev.* 2025, 531:216520.

[95] Mohan B, Rucman S, Singjai P, Pombeiro AJ, Sun W, *et al.* Advanced electrochemiluminescent approaches for contaminant detection in food matrices using metal-organic framework composites. *Food Chem.* 2025, 470:142625.

[96] Fu Z, He Y, Yang G, Yang J, Yuan R, *et al.* Carbohydrazide-induced low triggering potential electrochemiluminescence from perylene-based metal-organic framework for bioanalysis. *Biosens. Bioelectron.* 2025, 289:117887.

[97] Wang X, Xie Y, Zhang F, Xia J, Wang Z. Novel mesoporous mof nanoreactor based on modulator-induced defect formation strategy for electrochemiluminescence detection of miRNA-522. *Chem. Eng. J.* 2025, 513:162797.

[98] Zhao L, Xu Z, Song X, Ding C, Ju H. Self-supplying coreactant radical and structural distortion induced by carbonate ligand in metal-organic framework for anomalous deep-red self-electrochemiluminescence. *Chem. Sci.* 2025, 16(27):12493–12498.

[99] Xie J, Yang G, Yuan R, Chen S. A dual mode biosensor based on self-enhanced polyfluorene nanomaterial for fluorescence and electrochemiluminescence detection of tau protein. *Biosens. Bioelectron.* 2025, 271:117055.

[100] Li J, Fang J, Zhang R, Yang D, Duan A, *et al.* 2D conjugated polymer nanosheets: a new choice for boosting electrochemiluminescence. *Adv. Funct. Mater.* 2026, 36(22):e21938.

[101] Zhou S, Zhou T, Hou Y, Li W, Shen Y, *et al.* Recent advances in electrochemiluminescence based on polymeric luminophores. *Chin. Chem. Lett.* 2025, 36(5):110284.

[102] Wang Y, Wang R, Xu D, Tian M, Chen L, *et al.* Enhanced aggregation-induced electrochemiluminescence enabled by tuned molecular rigidity and rotatability for highly sensitive detection of lithium ions. *Anal. Chem.* 2026, 98(6):4995–5004.

[103] Li W, Liang Z, Wang P, Li Z, Ma Q. CuS@Ag heterostructure-based surface plasmonic coupling electrochemiluminescence sensor for glioma miRNA-124-3p detection. *Biosens. Bioelectron.* 2025, 274:117202.

[104] Wang C, Li M, Li Y, Hu X, Li C, *et al.* Aggregation-induced resonance energy transfer in polymer dots to boost electrochemiluminescence performance for bioimaging of glycan on cells. *Adv. Sci.* 2026, 13(19):e24265.

[105] Li C, Yang Z, Wang J, Cheng H, Liu J, *et al.* Nanoconfinement-enhanced aggregation-induced electrochemiluminescence for smartphone-adopted imaging analysis of cTnI. *Adv. Funct. Mater.* 2025, 35(35):2504380.

[106] Li S, Wang P, Ma Q. Recent progress and challenges in ECL biosensors for the identification of small extracellular vesicle and clinical diagnosis. *TrAC Trends Anal. Chem.* 2025, 189:118253.

[107] Cox M, January J, Mokwebo KV, Yussuf ST, Sanga NA, *et al.* Advances on electrochemiluminescent biosensors for TB biomarkers. *ACS Sens.* 2025, 10:2409–2430.

[108] Ge J, Yin T, Zhang H, Cao Y, Liu J, *et al.* Photo-crosslinking of doped magic-sized nanoclusters for the construction of enhanced electrochemiluminescence biosensors. *Chem. Sci.* 2025, 16(8):3671–3679.

[109] Bushira FA, Gao Z, Dong H, Jin Y. Electrochemiluminescence coordination systems: recent advances for sensing, imaging and biomedical applications. *Coord. Chem. Rev.* 2026, 557:217738.

[110] Wang X, Cao Z, Li H, Zhao S, Wang C, *et al.* Recent advances in single-atom catalysts-based electrochemiluminescence sensors. *Coord. Chem. Rev.* 2026, 546:217066.

[111] Dong X, Wu T, Li J, Li Y, Li J, *et al.* Crystalline porous frameworks for efficient electrochemiluminescence: from functional design to biosensing applications. *Coord. Chem. Rev.* 2026, 556:217692.

[112] Jiang S, Han Y, Zhang Y, Zhang C. Recent advances in label-free detection *in vitro* and label-free imaging *in vivo*. *Coord. Chem. Rev.* 2026, 549:217327.

[113] Feng Y, Wang C, Zhou W, Yang X, Paolucci F, *et al.* Tomography electrogenerated chemiluminescence imaging from magnetic microbeads. *Small* 2025, 21(22):e2500804.

[114] Zhang J, Ye D, Xu C, Sun X, Zhang W, *et al.* Super-resolved mapping of electrochemical reactivity in single 3D catalysts. *Nano Lett.* 2025, 25(5):2074–2081.

[115] Wang J, Li Y, Yang Q, Chauvin J, Cosnier S, *et al.* Crystalline energy funneling in mixed-ligand Zr-MOFs drives radical-triggered ECL amplification for ultrasensitive thrombin sensing. *ACS Sens.* 2025, 10(10):8090–8097.

[116] Jovic M, Prim D, Paciotti G, Pfeifer ME. Engineering a diagnostic platform based on a spatially resolved electrochemiluminescence immunoassay for low-plex biomarker detection at point-of-care: Mild traumatic brain injury and cardiac applications. *Lab Chip* 2025, 25(21):5428–5438.

[117] Shen Z, Chen Y, Chai Y, Liu J, Yuan R. Entire near-infrared-I electrochemiluminescence enhancement of gold nanoclusters. *Angew. Chem. Int. Edit.* 2025, 64(35):e202509884.

[118] Du Y, Zhu M, Song L, Pan T, Cui L, *et al.* Potassium-based metal-organic framework with coordination-induced electrochemiluminescence for biosensing applications. *Adv. Funct. Mater.* 2026, 36(3):e13294.

[119] Dai L, Fang J, Jiang T, Li Q, Ren X, *et al.* Multicomponent supramolecular nanoaggregates with co-emissive electrochemiluminescence. *Matter* 2025, 8(6):102056.

[120] Song H, Zou S, He Y, Luobu M, Han Z, *et al.* Surface-defect engineered benzothiazole nanoparticles for amplified electrochemiluminescence: monitoring charge transfer kinetics and ultrasensitive biosensing. *Adv. Funct. Mater.* 2026, 36(23):e20860.

[121] Cao Y, Wang J, Lin C, Geng Y, Ma C, *et al.* Zwitterionic electrochemiluminescence biointerface contributes to label-free monitoring of exosomes dynamics in a fluidic microreaction device. *Adv. Funct. Mater.* 2023, 33(18):2214294.

[122] Chen J, Wu T, Du Y, Zhao H, Wu D, *et al.* Iron-doped cobalt molybdate enhanced electrochemiluminescence imaging for dynamic multilevel information encryption system construction and biomarker sensing analysis. *Angew. Chem. Int. Edit.* 2025, 137(27):e202507426.

[123] Cao Y, Zhang L, Song H, Yang X, Gao Y, *et al.* Engineering Pt-Ni alloy coral nanoclusters with efficient oxygen reduction: Enabling endogenous oxygen-mediated sustainable electrochemiluminescence for breast cancer diagnosis. *Adv. Funct. Mater.* 2026, 36(20):e21284.

[124] Shi B, Ru Z, Jia D, Du Y, Hu L, *et al.* Host-guest confinement in post-metallized COFs for enhanced electrochemiluminescence coupled with y-shaped DNA amplification for microrna-499 detection. *Biosens. Bioelectron.* 2026, 304:118623.

[125] Tang X, Peng X, Zhang W, Li Z, He M, *et al.* Ultrasensitive electrochemiluminescence nanoprobe for early screening and early diagnosis of cervical cancer. *Anal. Chem.* 2026, 98(11):8550–8561.

[126] Li X, Xia M, Peng K, Xiang Y, Liu K, *et al.* Application of an l-cysteine-enhanced Ag NCs@C NF amplification-free ECL biosensor for miRNA. *Anal. Chem.* 2026, 98(6):4666–4674.

[127] Wang Q, Sheng M, Zheng Y, Zhang B, Jin Z, *et al.* Electrochemiluminescence biosensing platform based on CRISPR/Cas12a and DNA nanotweezer-mediated catalytic hairpin assembly amplification. *Anal. Chem.* 2026, 98(13):9832–9841.

[128] Yang B, Yang W, Chen F, Song Z, Chen X, *et al.* Bipolar electrochemiluminescence detection of ampicillin resistance genes via HRCA-mediated precipitation-induced conductivity modulation. *Anal. Chem.* 2025, 97(25):13707–13714.

[129] Wu Y, Ye Z, Chen Y, Zhang Y, Liu R, *et al.* DNA-engineered CsPbBr(3) superlattices with enhanced electronic coupling for high-performance electrochemiluminescence biosensing. *ACS Sens.* 2025, 10(8):6231–6240.

[130] Li Y, Li J, Zhu D, Wang J, Shu G, *et al.* 2D Zn-porphyrin-based Co(II)-MOF with 2-methylimidazole sitting axially on the paddle-wheel units: an efficient electrochemiluminescence bioassay for SARS-CoV-2. *Adv. Funct. Mater.* 2022, 32(48):2209743.

[131] Qin J, Zhou J, Chen J, Gu P, Wang Y, *et al.* Intramolecular switching oxygen reduction reaction driven by dual-crystalline bimetallic mof induces self-potential-resolved electrochemiluminescence biosensor. *Angew. Chem. Int. Edit.* 2025, 64(29):e202508627.

[132] Dong Y, Fu B, Wu H, Jie G. Single-electrode high-throughput 12-well array electrochemiluminescence imaging sensor for portable parallel dual-color analysis of dual breast cancer susceptibility genes. *Anal. Chem.* 2026, 98(7):5593–5602.

[133] Yang H, Zheng J, Wang W, Lin J, Wang J, *et al.* Zr-MOF carrier-enhanced dual-mode biosensing platforms for rapid and sensitive diagnosis of mpox. *Adv. Sci.* 2024, 11(38):2405848.

[134] Xiong H, Zhu C, Dai C, Ye X, Li Y, *et al.* An alternating current electroosmotic flow-based ultrasensitive electrochemiluminescence microfluidic system for ultrafast monitoring, detection of proteins/mirnas in unprocessed samples. *Adv. Sci.* 2024, 11(6):2307840.

[135] Xu P, Sun N, Cao X, Xie H, Zuo Y, *et al.* Curved pi-conjugated dehydrobenzoannulene as an electron acceptor enabling fluorescence and electrochemiluminescence emission. *Org. Lett.* 2025, 27(12):2868–2872.

[136] Shi X, Jiao L, Zong P, Jia X, Chen C, *et al.* Single-atom cobalt sites efficient activation of H_2O_2 with enhanced O_2 tolerance for electrochemiluminescence sensing of plasticizers. *Small* 2025, 21(34):2504692.

[137] Ni J, Xiong Y, Zhang G, Chen X, Lin Z, *et al.* Bimetallic-doped metal-organic gel for efficient electrochemiluminescence: Staircase-mediated energy transfer and applications in epinephrine detection. *Anal. Chem.* 2025, 97(35):19111–19118.

[138] Xiang L, Hou Y, Li W, Wu K, Wang K, *et al.* Boosting electrochemiluminescence of carbon nitrides via molecular capacitor-mediated spatiotemporal electron coordination. *Adv. Sci.* 2026, 13(3):e06277.

[139] Li X, Sun H, Zong L, Xie P, Cosnier S, *et al.* Molecularly engineered pi-electron relay enables coreactant-free, oxygen-driven electrochemiluminescence. *Biosens. Bioelectron.* 2026, 299:118464.

[140] Song S, Liu W, Bao J, Zhu H, Wang A, *et al.* Photodynamic-assisted electrochemiluminescence enhancement toward advanced BODIPY for precision diagnosis of Parkinson. *Anal. Chem.* 2024, 96(21):8586–8593.

[141] Sun N, Ding J, Jia H, Xie H, Zhang J, *et al.* Synthesis of carbazole-based electron donor-acceptor architectures enabling ultrasensitive epinephrine detection. *Org. Lett.* 2025, 27(46):12779–12783.

[142] Wang Z, Cao W, Yuan R, Wang H. High AIECL performance of tetraphenylethene derivatives originated from the linear increasing of benzene ring and solvent regulation for sensitive measurement of melatonin. *Biosens. Bioelectron.* 2023, 237:115544.

[143] Zhu Z, Zeng C, Zhao Y, Ma J, Yao X, *et al.* Precise modulation of intramolecular aggregation-induced electrochemiluminescence by tetraphenylethylene-based supramolecular architectures. *Angew. Chem. Int. Edit.* 2023, 135(46):e202312692.

[144] Ouyang X, Wu Y, Guo L, Li L, Zhou M, *et al.* Self-assembly induced enhanced electrochemiluminescence of copper nanoclusters using DNA nanoribbon templates. *Angew. Chem. Int. Edit.* 2023, 135(21):e202300893.

[145] Yang Q, Deng J, Zhu D, Yu F, Li Y, *et al.* Energy-level rule guided construction of low-coordinated lnofs for redox-gated and programmable low-bias electrochemiluminescence. *Adv. Funct. Mater.* 2026, 36(25):e25510.

[146] Li J, Xi M, Hu L, Sun H, Zhu C, *et al.* A controlled release aptasensor utilizing AIE-active MOFs as high-efficiency ECL nanoprobe for the sensitive detection of adenosine triphosphate. *Anal. Chem.* 2024, 96(5):2100–2106.

[147] Knezevic S, Totoricaguena-Gorrino J, Gajjala RKR, Hermenegildo B, Ruiz-Rubio L, *et al.* Enhanced electrochemiluminescence at the gas/liquid interface of bubbles propelled into solution. *J. Am. Chem. Soc.* 2024, 146(32):22724–22735.

[148] Li J, Zhang R, Deng S, Zhang N, Yang D, *et al.* Multifunctional PTCA/GO for a glucose-driven electrochemiluminescence biosensor. *Nano Lett.* 2025, 25(41):15141–15149.

[149] Nie W, Jiang J, Wei X, Zhuo L, Li D, *et al.* An all-soft wearable electrochemiluminescence chip for sweat metabolite detection. *Adv. Sci.* 2026, 13(10):e19435.

[150] Liu M, Liu M, Chen W, Li F, Cai S, *et al.* Identifying N coordination types of single-atom catalysts by spin-modulated luminol cathodic electrochemiluminescence. *Angew. Chem. Int. Edit.* 2025, 137(11):e202421755.

[151] Huang X, Shen L, Qu W, Xu Y, Fu W, *et al.* Microcavity-enhanced directional electrochemiluminescence output from single molecular crystals. *J. Am. Chem. Soc.* 2025, 147(34):30777–30784.

[152] Zhang Z, Zhang F, Cui Y, Luo W, Shu M, *et al.* Imaging and tailoring chemical evolution kinetics of (0001) facet on single beta-$Co(OH)_2$ nanoplates for the electrocatalytic oxygen evolution reaction. *J. Am. Chem. Soc.* 2025, 147 (27):23617–23624.

[153] Zhu W, Dong J, Ruan G, Zhou Y, Feng J. Quantitative single-molecule electrochemiluminescence bioassay. *Angew. Chem. Int. Edit.* 2023, 62(7):e202214419.

[154] Wang Y, Liu T, Yu S, Luo R, Bao S, *et al.* Polychromatic electrochemiluminescence imaging of single heteroligand metal-organic crystals. *Angew. Chem. Int. Edit.* 2025, 137(19):e202501151.
[155] Gou X, Manko H, Vidic J, Cognet L, Zhu J, *et al.* From microscale to nanoscale shadow electrochemiluminescence microscopy. *Angew. Chem. Int. Edit.* 2026, 138(18):e21654.
[156] Layman BR, Hill ML, Carrel DM, Nguyen JH, Dick JE. Exploring the mechanism of microdroplet explosion on an electrified interface. *J. Am. Chem. Soc.* 2026, 148(2):2629–2638.
[157] Li J, Xu Y, Cao Z, Qu W, Guo W, *et al.* Tuning electrochemiluminescence color through single molecular crystals. *Adv. Funct. Mater.* 2026:e26171.
[158] Shi Y, Liu Y. Qualitative and quantitative electrochemiluminescence evaluation of trace pt single-atom in MXenes. *Nat. Commun.* 2024, 15(1):7086.
[159] Huang X, Shi Q, Lu Y, Li B, Ning Y, *et al.* Single-molecule electrochemiluminescence imaging of plasmonic hot spot reactivity. *Angew. Chem. Int. Edit.* 2025, 137(35):e202508266.
[160] Hill ML, Layman BR, Dick JE. Real-time visualization of an elusive, strong reducing agent during tris(2,2'-bipyridyl)ruthenium(ii) electro-oxidation in water. *J. Am. Chem. Soc.* 2025, 147(21):17701–17709.
[161] Wang Y, Zhou S, Zheng Y, Wang Y, Hou Y, *et al.* Measurements of local pH gradients for electrocatalysts in the oxygen evolution reaction by electrochemiluminescence. *J. Am. Chem. Soc.* 2025, 147(22):19380–19390.
[162] Altschuler SJ, Wu L. Cellular heterogeneity: do differences make a difference? *Cell* 2010, 141(4):559–563.
[163] Carter B, Zhao K. The epigenetic basis of cellular heterogeneity. *Nat. Rev. Genet.* 2021, 22(4):235–250.
[164] Geiler-Samerotte KA, Bauer CR, Li S, Ziv N, Gresham D, *et al.* The details in the distributions: Why and how to study phenotypic variability. *Curr. Opin. Biotechnol.* 2013, 24(4):752–759.
[165] Zhang H, Jiang H, Liu X, Wang X. A review of innovative electrochemical strategies for bioactive molecule detection and cell imaging: current advances and challenges. *Anal. Chim. Acta* 2024, 1285:341920.
[166] Ding H, Su B, Jiang D. Recent advances in single cell analysis by electrochemiluminescence. *ChemistryOpen* 2023, 12(5):e202200113.
[167] Yang Q, Huang X, Gao B, Gao L, Yu F, *et al.* Advances in electrochemiluminescence for single-cell analysis. *Analyst* 2023, 148(1):9–25.
[168] Li L, Yu S, Wu J, Ju H. Regulation of target-activated CRISPR/Cas12a on surface binding of polymer dots for sensitive electrochemiluminescence DNA analysis. *Anal. Chem.* 2023, 95(18):7396–7402.
[169] Richter MM. Electrochemiluminescence (ECL). *Chem. Rev.* 2004, 104(6):3003–3036.
[170] Li L, Chen W, Hu X, Tang Z, Wang C, *et al.* Coupled poly(ethylenimine) coreactant to enhance electrochemiluminescence of polymer dots for array imaging of protein biomarkers. *Anal. Chem.* 2024, 96(10):4308–4313.
[171] Miao W. Electrogenerated chemiluminescence and its biorelated applications. *Chem. Rev.* 2008, 108(7):2506–2553.
[172] Liu Z, Qi W, Xu G. Recent advances in electrochemiluminescence. *Chem. Soc. Rev.* 2015, 44(10):3117–3142.

[173] Paciorek T, Zažímalová E, Ruthardt N, Petrášek J, Stierhof YD, *et al.* Auxin inhibits endocytosis and promotes its own efflux from cells. *Nature* 2005, 435(7046):1251–1256.
[174] Zhang J, Wang X, Xie Y, Chao J, Huang W. Recent progress of electrochemiluminescence imaging for single-entity analysis. *Adv. Mater. Technol.* 2026, 11(2):e01392.
[175] Zahn H, Steif A, Laks E, Eirew P, VanInsberghe M, *et al.* Scalable whole-genome single-cell library preparation without preamplification. *Nat. Methods* 2017, 14(2):167–173.
[176] Tan WK, Lin Q, Lim TM, Kumar P, Loh CS. Dynamic secretion changes in the salt glands of the mangrove tree species Avicennia officinalis in response to a changing saline environment. *Plant Cell Environ.* 2013, 36(8):1410–1422.
[177] Zelanis A, Barcick U, Racorti NDV, Salardani M. Heterotypic communication as the promoter of phenotypic plasticity of cancer cells: The role of cancer secretomes. *Proteomics* 2023, 23(23–24):2200243.
[178] Zhang J, Jin R, Chen Y, Fang D, Jiang D. Enhanced electrochemiluminescence at single lithium iron phosphate nanoparticles for the local sensing of hydrogen peroxide efflux from single living cell under a low voltage. *Sens. Actuators B Chem.* 2021, 329:129208.
[179] Li X, Qin X, Wang Z, Wu Y, Wang K, *et al. In situ* imaging of endogenous hydrogen peroxide efflux from living cells via bipolar gold nanoelectrode array and electrochemiluminescence technology. *ACS Sens.* 2022, 7(8):2446–2453.
[180] Ding H, Guo W, Ding L, Su B. Confined electrochemiluminescence at microtube electrode ensembles for local sensing of single cells. *Chin. J. Chem.* 2021, 39(10):2911–2916.
[181] Wang N, Ao H, Xiao W, Chen W, Li G, *et al.* Confined electrochemiluminescence imaging microarray for high-throughput biosensing of single cell-released dopamine. *Biosens. Bioelectron.* 2022, 201:113959.
[182] Han D, Jiang M, Pan R. Spatial visualization of secreted lysyl oxidase activity from single living cells via label-free electrochemiluminescence microscopy. *Chem. Biomed. Imaging.* 2025, 4(4):602–609.
[183] Zhou J, Liu Y. *In situ* interface reaction-enabled electrochemiluminescence imaging for single-cell formaldehyde release analysis. *Sens. Diagn.* 2024, 3(9):1571–1578.
[184] Hiramoto K, Ino K, Komatsu K, Nashimoto Y, Shiku H. Electrochemiluminescence imaging of respiratory activity of cellular spheroids using sequential potential steps. *Biosens. Bioelectron.* 2021, 181:113123.
[185] Yu S, Hu X, Pan J, Lei J, Ju H. Nanoconfined cathodic electrochemiluminescence for self-sensitized bioimaging of membrane protein. *Anal. Chem.* 2023, 95:16593–16599.
[186] Jiang S, Han Y, Zhang Y, Zhang C. Recent advances in label-free detection *in vitro* and label-free imaging *in vivo*. *Coord. Chem. Rev.* 2026, 549:217327.
[187] Wang C, Wang Y, Liu J, Li F, Gai P. Nanozyme-based biofuel cell ingeniously coupled with luminol chemiluminescence system through *in situ* co-reactant generation for dual-signal biosensing. *Anal. Chem.* 2023, 95(42):15763–15768.
[188] Guo X, Zhu K, Zhu X, Zhao W, Miao Y. Two-dimensional molecular condensation in cell signaling and mechanosensing. *Acta Biochim. Biophys. Sin.* 2023, 55(7):1064.
[189] Zhang H. Mechanism associated with aberrant lncRNA MEG3 expression in gestational diabetes mellitus. *Exp. Ther. Med.* 2019, 18(5):3699–3706.

[190] Hou W. Krt17: a key driver of cancer therapy resistance and emerging therapeutic target. *Cancer Manag. Res.* 2025, 17:2705–2717.

[191] Tehrani HA, Zangi M, Fathi M, Vakili K, Hassan M, *et al.* GPC-3 in hepatocellular carcinoma; a novel biomarker and molecular target. *Exp. Cell Res.* 2025, 444(2):114391.

[192] Sehar T, Wei G, Kainat, Zulqurnain, Iqra, *et al.* Recent proceedings of advanced electrochemiluminescence imaging technology and applications in accurate analysis. *Chem. Biomed. Imaging* 2025, 4(4):485–509.

[193] Wang N, Gao H, Li Y, Li G, Chen W, *et al.* Dual intramolecular electron transfer for *in situ* coreactant-embedded electrochemiluminescence microimaging of membrane protein. *Angew. Chem. Int. Edit.* 2021, 60(1):197–201.

[194] Chen Y, Gou X, Ma C, Jiang D, Zhu J. A synergistic coreactant for single-cell electrochemiluminescence imaging: guanine-rich ssDNA-loaded high-index faceted gold nanoflowers. *Anal. Chem.* 2021, 93(21):7682–7689.

[195] Zhang J, Hao L, Chao J, Wang L, Su S. Enhanced electrochemiluminescence imaging of single cell membrane proteins based on Co_3O_4 nanozyme catalysis. *Chem. Commun.* 2023, 59(78):11736–11739.

[196] Gou X, Zhang Y, Xing Z, Ma C, Mao C, *et al.* Site-selective heat boosting electrochemiluminescence for single cell imaging. *Chem. Sci.* 2023, 14:9074–9085.

[197] Zhang H, Liu Y, Yao M, Han W, Zhang S. Cathodic electrochemiluminesence microscopy for imaging of single carbon nanotube and nucleolin at single tumor cell. *Anal. Chem.* 2023, 95(2):570–574.

[198] Zhang J, Jin R, Jiang D, Chen H. Electrochemiluminescence-based capacitance microscopy for label-free imaging of antigens on the cellular plasma membrane. *J. Am. Chem. Soc.* 2019, 141(26):10294–10299.

[199] Schirripa Spagnolo C, Moscardini A, Amodeo R, Beltram F, Luin S. Quantitative determination of fluorescence labeling implemented in cell cultures. *BMC Biol.* 2023, 21(1):190.

[200] Wang Y, Jin R, Sojic N, Jiang D, Chen H. Intracellular wireless analysis of single cells by bipolar electrochemiluminescence confined in a nanopipette. *Angew. Chem. Int. Edit.* 2020, 132(26):10502–10506.

[201] Li B, Lu Y, Huang X, Sojic N, Jiang D, *et al.* Stimuli-responsive DNA nanomachines for intracellular targeted electrochemiluminescence imaging in single cells. *Angew. Chem. Int. Edit.* 2025, 137(6):e202421658.

[202] Wang Y, Jiang D, Chen H. Wireless electrochemical visualization of intracellular antigens in single cells. *CCS Chemistry* 2022, 4(7):2221–2227.

[203] Ma C, Wu S, Zhou Y, Wei H, Zhang J, *et al.* Bio-coreactant-enhanced electrochemiluminescence microscopy of intracellular structure and transport. *Angew. Chem. Int. Edit.* 2021, 1133(9):4957–4964.

[204] Ma Y, Colin C, Descamps J, Arbault S, Sojic N. Shadow electrochemiluminescence microscopy of single mitochondria. *Angew. Chem. Int. Edit.* 2021, 133:18890–18897.